OPEN ACCESS
IOP Publishing | Songshan Lake Materials Laboratory
Materials Futures
Mater. Futures 1 (2022) 042102 (20pp)
https://doi.org/10.1088/2752-5724/ac9248

Topical Review

Bilayer metal halide perovskite for efficient and stable solar cells and modules

Yanqing Zhu[1], Min Hu[2,*], Mi Xu[3], Bo Zhang[4], Fuzhi Huang[3,5], Yi-Bing Cheng[3,5] and Jianfeng Lu[1,3,*]

[1] State Key Laboratory of Silicate Materials for Architectures, Wuhan University of Technology, Wuhan 430070, People's Republic of China
[2] School of Electronic and Electrical Engineering, Hubei Province Engineering Research Centre for Intelligent Micro-Nano Medical Equipment and Key Technologies, Wuhan Textile University, Wuhan 430200, People's Republic of China
[3] Foshan Xianhu Laboratory of the Advanced Energy Science and Technology Guangdong Laboratory, Foshan 528216, People's Republic of China
[4] Shanxi Lu'An Photovoltaics Technology Co., Ltd, Changzhi 046011, People's Republic of China
[5] State Key Laboratory of Advanced Technology for Materials Synthesis and Processing, Wuhan University of Technology, Wuhan 430070, People's Republic of China

E-mail: hm@wtu.edu.cn and jianfeng.lu@whut.edu.cn

Received 21 July 2022, revised 29 August 2022
Accepted for publication 14 September 2022
Published 25 October 2022

Abstract

To reach the target of carbon neutral, a transition from fossil energy to renewable energy is unavoidable. Photovoltaic technology is considered one of the most prominent sources of renewable energy. Recently, metal halide perovskite materials have attracted tremendous interest in the areas of optoelectronic devices due to their ease of processing and outstanding performance. To date, perovskite solar cells (PSCs) have shown high power conversion efficiency up to 25.7% and 31.3% for the perovskite-silicon tandem solar cells, which promises to revolutionize the PV landscape. However, the stability of PSCs under operating conditions has yet to match state-of-the-art silicon-based solar cell technology, in which the stability of the absorbing layer and relevant interfaces is the primary challenge. These issues become more serious in the larger area solar modules due to the additional interfaces and more defects within the perovskite. Bilayer perovskite film composed of a thin low dimensional perovskite layer and a three-dimensional perovskite layer shows great potential in fabricating solar cells with high efficiency and stability simultaneously. In this review, recent advancements, including composition design and processing methods for constructing bilayer perovskite films are discussed. We then analyze the challenges and resolutions in deposition bilayer perovskite films with scalable techniques. After summarizing the beneficial effect of the bilayer structure, we propose our thinking of feasible strategies to fabricate high efficiency perovskite solar modules

* Authors to whom any correspondence should be addressed.

with a long lifetime. Finally, we outline the directions for future work that will push the perovskite PV technology toward commercialization.

Keywords: perovskite solar cell, perovskite solar module, bilayer, stability, scalable technique

(Some figures may appear in colour only in the online journal)

1. Introduction

Metal halide perovskites, with the merits of being solution-processable and having tunable bandgaps, high carrier mobility, high absorption coefficients, and superior charge-transfer properties, are widely used in different areas, such as solar cells, light-emitting diodes (LEDs), lasers, and detectors. As one of the most promising photovoltaic technologies, the power conversion efficiency (PCE) of perovskite solar cells (PSCs) has reached 25.7%. The larger area perovskite solar modules (PSMs) have been demonstrated to be efficient with a size of 804 cm^2, reaching an efficiency of 17.9% [1]. However, the available strategies for fabricating high performing PSMs that can withstand environmental stimuli, such as heat, humidity and irradiation, are limited. Many efforts have been endowed to improve their stability, such as composition engineering [2], interface modification [3–5], encapsulation [6–8], and adjustment of tolerance factors [9]. Recently, it is noticed that covering the three dimensional (3D) perovskite with a layer of low-dimensional material, i.e. vertical heterostructure, has been used to improve both the efficiency and stability of PSCs [10–12].

3D hybrid perovskite materials generally have a formula of ABX_3, where A stands for a monovalent cation (e.g. formamidinium, FA^+; methylammonium, MA^+; caesium ion, Cs^+, etc), B stands for a metal ion (e.g. lead ion, Pb^{2+}; tin ion, Sn^{2+}; germanium ion, Ge^{2+}, etc) and X is a halide anion (e.g. chloride, Cl^-; bromide, Br^-; iodide, I^-, etc) [13]. It consists of continuous corner-sharing metal halide $[BX_6]^{4-}$ octahedra, where the metal and halogen atoms are located in the center and the vertexes of the octahedral unit, respectively, while organic or inorganic cations fill the space between eight octahedral cells to balance crystal charges. It conforms to the formula:

$$t = \frac{R_A + R_X}{\sqrt{2}(R_B + R_X)}, \mu = R_B/R_X \quad (1)$$

where the R_A, R_B and R_X are the radius of the A, B, X, respectively. t is the tolerance factor and μ is the octahedral factor [9]. In order to maintain a 3D structure, t and μ should satisfy $0.8 < t < 1.0$ and $0.44 < \mu < 0.90$ [13, 14], respectively.

When the tolerance factor is larger than 1.0, the inorganic lead halogen layer transforms to layered, angular shared or isolated octahedron structure. 2D perovskites are considered as sheets or layers that split from 3D perovskites in specific crystallographic directions. The single-angular or multi-angular shared layer is determined by the organic cation, forming Ruddlesden–Popper or Dion–Jacobson perovskite [15]. The general chemical formula of 2D perovskite is A_2BX_4 [16, 17]. In 1D perovskite, the metal halide octahedron is angular, edge-shared, or surface-shared and surrounded by organic cations. Their configurations could be either linear or zigzag, and their chemical formulas are variable according to the connection styles and the organic cations [18]. The general chemical formula of 0D perovskite is A_4BX_6 [19], in which the metal halide octahedral anions or metal halide clusters are completely surrounded and separated by organic cations [18, 19]. These molecular perovskite units are strictly and periodically embedded in the crystal lattice together with organic cations to form bulk materials. Overall, by selecting appropriate organic cations and metal halides, the structure of halide perovskite can be finely controlled to show different sizes at the molecular level, forming 0D, 1D, 2D, or 3D structure (figures 1(a)–(d)) [20].

In comparison with 3D perovskites, low-dimensional (0D, 1D, 2D) perovskites have a wider range of structures, lower self-doping, higher lattice formation energy, superior moisture stability, and higher ion migration activation energy etc [21–23]. For example, large organic cations in 2D perovskite, (e.g. phenylethylammonium, PEA^+), can effectively block the accessible pathway of moisture or oxygen invasion, passivate the defects at grain boundaries, and suppress the ion migration, thus improve the stability of PSCs [24]. However, perovskites with 2D structure are generally not a good choice for high-performance solar cells due to their wide optical bandgap, low carrier mobility, and large binding energy [25, 26].

Figure 1(e) shows the configuration of a *n–i–p* PSC based on 3D/2D bilayer perovskite films. It has been demonstrated that it not only can retain the superior optoelectronic properties of 3D perovskite but also inherit the good stability of low-dimensional perovskite. Figure 1(f) summarizes the efficiency evolution of small cells (<1 cm^2), mini-module (10–200 cm^2) and submodule (200–800 cm^2) in recent years. It is noticed that most of the efficiency records of small-area cells are created by using bilayer perovskite. Figure 1(g) summarizes the reported lifetimes of cells and modules based on single layer or bilayer perovskite films. The T_{90} (the time over which the device efficiency reduces to 90% of its initial value) of small area cells reaches 5 years (2000 h sunshine duration per year), while it is *ca.* 1200 h for mini-modules under continuous operation [73, 82]. The difference in lifetimes between cells and modules is large, which both clearly lag behind the commercialized PV products [49]. Perovskite PV technology will undergo relentless scrutiny for long-term stability before entering the market.

Future perspectives

Photovoltaic technology is a key driver for achieving the ambitious energy targets of carbon neutral. Metal halide perovskite solar cells (PSCs) have become the central focus of the photovoltaic field in recent years. With a superior photovoltaic performance versus cost ratio compared to its rivals (e.g. silicon, GaAs solar cells), this new type of solar cell promises to revolutionize the PV landscape. The transition from research to industrial production of PSCs requires further progress in both stability, efficiency and scalability—three elements that often display an inverse inter-dependency. The bilayer structure of perovskite shows great potential in achieving both high efficiency and stability, though most of the advancements are based on mm-size devices. The future directions of the bilayer perovskite include the following points: (a) the possibility of fabricating large area devices is the most attractive point of perovskite technology. Therefore, scalable deposition methods for bilayer perovskite are needed; (b) in order to simultaneously inherit the advantages of low-dimensional and three-dimensional perovskites while avoiding their disadvantages, treating the bilayer as a functional motif may not only lead to the above requirements, but also lead to more disruptive properties; (c) most morphology studies of bilayer perovskite are based on routine techniques, which are actually not feasible for ultrathin layers. A deep study of the morphology with more advanced techniques is needed.

In this review, we first introduce the deposition strategy that is commonly used for constructing bilayer perovskite films, in which the challenges for depositing larger area films are proposed and discussed. After having this knowledge, the beneficial effects, including the enhanced stability and photovoltaic performance obtained by employing 3D/2D bilayer perovskite are summarized and prospected. Finally, we propose a perspective on the future direction of bilayer perovskite for larger area modules with both high efficiency and stability.

2. The process for bilayer perovskite

In this part, we summarize the deposition strategy for bilayer perovskite thin film, in which low-dimensional perovskite layer will be focused. Table 1 summarizes some of the most popular organic ammonium salts used for 3D/low-dimensional bilayer perovskite films. Larger size groups, such as alkyl chains, functionalized aromatics are commonly chosen to build the low-dimensional perovskite. These ammonium salts are usually highly soluble in anti-solvents, such as isopropanol (IPA), chlorobenzene (CB), which are reported to be inert to perovskite. Therefore, many solution processes, such as spin-coating, blade coating, slot die coating are available for the low-dimensional perovskite layer deposition. As shown in figure 2, the deposition process for low-dimensional perovskite can be categorized to wet and dry methods, including *in-situ* growth method, immersion, anti-solvent method, vapor deposition, hot pressing, and other methods.

2.1. In-situ *growth method*

In-situ growth is the most commonly used method to prepare low-dimensional perovskite layer. For example, it can be obtained by spin-coating a solution containing organic ammonium salt on the surface of the 3D perovskite film, or soaking the 3D perovskite film into the solution (figure 2). The salts react with PbI_2 or even perovskite on the surface to form low-dimensional perovskite, thus covering its surface and resulting of 3D/low-dimensional bilayer. With this bilayer structure, devices with high open-circuit voltage (V_{OC}) and the efficiency can be fabricated. Zhang *et al* spin-coated a precursor containing N, N-dimethyl-1,3-propane diammonium iodine on 3D perovskite thin film. The cells based on this bilayer perovskite showed a champion efficiency of 24.7% [38]. Similarly, 3D/1D bilayer perovskite can also be prepared by *in-situ* growth method. For instance, Kaneko *et al* spin-coated 4-*tert*-butylpyridinium iodide on a 3D perovskite film, forming 1D perovskite $TBPPbI_3$ on the top [89]. Since the carrier mobility and binding energy of low-dimensional perovskite are relatively lower, therefore the morphology, such as the crystallinity, thickness, phase, film coverage of the low-dimensional perovskite are critical important for the device performance [90].

Solvent, concentration and annealing process are the three major factors determining the morphology thus the optoelectronic properties of bilayer perovskite film (figure 3(a)). To avoid the damage of 3D perovskite film, anti-solvents such as IPA [10, 12] or CB [61, 64] are commonly used for the 2D precursor due to the low solubility for 3D perovskites. However, Yoo *et al* found that IPA can also slightly dissolve the 3D perovskite even in a short time (< 2 s) due to its high polarity and the tendency of forming hydrogen bonds with perovskite. Therefore, non-hygroscopic solvents such as chloroform, or hexaflfluoro-2-propanol are suggested (see figures 3(b) and (c)) [27]. Cho *et al* suggested a dynamic spin-coating method when IPA is used, which results of a thinner and more uniform bilayer film [91]. Concentration of ammonium salt is another major factor. He *et al* found that when the concentration of *n*-BAI is too high (> 1 mg ml^{-1}), the 2D layer will be too thick, which impedes the interfacial charge extraction, thus reduce the short-circuit current density (J_{SC}) and fill factor (FF) of the devices [88]. In contrary, when the concentration is too low, the 2D layer is more like island instead of a continuous film, which decreases its resistance to moisture or other environment stimuli (figures 3(d)–(g)) [87]. Annealing process can affect the transformation of ammonium salt to 2D perovskite. As reported by He *et al*, 2D perovskites with high *n* values ($n > 3$, *n* is the number of inorganic layers) and even unreacted residual *iso*-pentylammonium iodide molecules can be detected. By adjusting the annealing temperature, this 3D/2D perovskite heterojunction composition

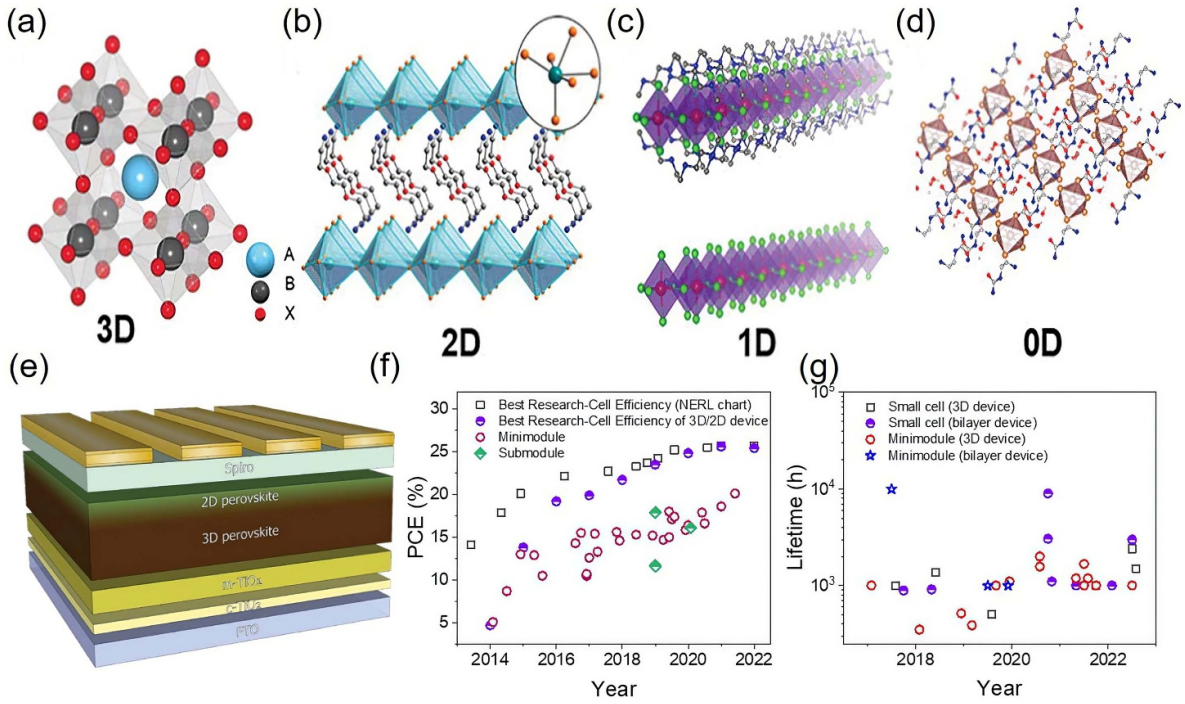

Figure 1. Typical crystal structure of metal halide perovskites: (a) 3D, (b) 2D, (c) 1D, (d) 0D. Reproduced from [20]. CC BY 4.0. (e) The configuration of 3D/2D bilayer perovskite based solar cells. Reproduced from [27]. CC BY 3.0. (f) PCE evolution of 3D perovskite solar cells (*black*), 3D/2D perovskite solar cells (*purple*), mini-module (*red*) and submodule (*green*). The data are based on published works [1, 28–64]. (g) The lifetimes of 3D or bilayer perovskite based solar cells and mini modules in recent years. The data are based on published works [29, 36, 38, 47, 53, 65–81].

can improve the charge extraction, suppress the interfacial ion defects, leading to a low bandgap-to-voltage loss (figure 3(h)) [88]. To minimize the thickness of the 2D layer while retain the continuous film morphology, Wei *et al* introduced a low concentration of 2-phenylethanamine hydroiodide (PEAI) into the anti-solvent (toluene or ethyl acetate) when depositing the 3D perovskite layer [92, 93]. The associated diffraction peaks of 2D perovskite appeared in the x-ray diffraction (XRD) spectra, suggesting the formation of 2D layer. Moreover, they found that PEA cations can permeate into the bulk film, which passivated the defects at grain boundaries and film surface simultaneously [93]. The results of contact potential difference suggested that the potential distribution of the bilayer film is more uniform in comparison with the film fabricated by conventional anti-solvent.

2.2. Solvent-free method

Solvent-free methods, such as vapor deposition and hot-press offer additional advantages in deposition of bilayer perovskite films, including the intrinsic purity of sublimed materials, no solvent is involved, control over the film thickness, and the low substrate-fabrication temperature, feasible on larger substrate size. In 2018, Li *et al* developed a low-pressure vapor-assisted method to construct the bilayer perovskite. In this method, a precursor containing PEAI and PbI_2 was firstly deposited on a TiO_2 substrate by spin-coating. Subsequently, films were transferred into an oven to react with MAI vapor at a low-pressure. The XRD and grazing-incidence wide-angle x-ray scattering (GIWAXS) results showed that quasi-2D single layer, 3D/2D bilayer and 3D single layer perovskites can be obtained by controlling the ratio of PEAI to PbI_2 [94]. Lin *et al* placed $MAPbI_3$ 3D perovskite and BAI powder in an oven with 120 °C to fabricate the bilayer films. The quality and transformation degree of 2D perovskite films can be controlled by adjusting the reaction time (figure 4(a)) [95]. When the reaction time is 5 min, the grains of $MAPbI_3$ emerged at both the surface and bulk, representing a partial transformation from 3D to 2D structure. After reacting for 60 min, the surface morphology changed to small crystals of thin sheet 2D perovskite while the bulk retains as 3D structure [95].

Dual-source vacuum deposition was used to prepare 3D/2D bilayer perovskites by La-Placa *et al.* Firstly, the 3D $MAPbI_3$ film was obtained by co-evaporation of MAI and PbI_2. Then, the sample was moved to another vacuum chamber to co-evaporate PEAI and PbI_2, thus forming a 2D layer on top of the 3D layer [96]. Jang *et al* prepared 3D/2D perovskite by solid-phase in-plane growth method. As shown in figure 4(b), they first physically stacked a solid 2D film and a 3D film, with surfaces contact each other. Then, heat and pressure are applied to induce a transfer of 2D layer from the stacked solid 2D film to the top of the 3D film. In the initial stage, 2D perovskite seeds are formed, and gradually grow along the in-plane direction of the 3D film, forming 3D/2D bilayer. After a specific pressing time, the original 2D solid precursors are separated and the complete 3D/2D bilayer is obtained. The scanning electron microscopy (SEM) images provides a glimpse of the reaction process [97].

Table 1. Examples of organic ammonium salts for bilayer perovskites and the corresponding device performance, values in brackets are the performance of modules.

Film structure	Chemical formula	Molecular structure of ammonium salt	Deposition method	Stability	Device configuration	V_{OC} (V)	PCE (%)	References.
3D/2D	Ethylammonium iodide (EAI)	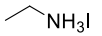	*In-situ* growth (solvent:IPA: DMF = 200:1v/v)	86% of initial PCE, 2000 h, 1sun, N_2 (encapsulated)	ITO|SnO_2-EDTAK|$Cs_{0.05}FA_{0.54}MA_{0.41}Pb(I_{0.98}Br_{0.02})_3$|EAMA| Spiro-OMeTAD/Au	1.12 (7.64)	21.8 (16.6)	[53]
	3-fluoro-phenethylammonium (3F-PEA)	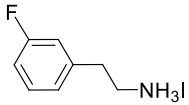	*In-situ* growth (solvent:IPA)	100% of initial PCE, 1000 h, 1sun, 50%RH (encapsulated)	ITO|NiOx|$Cs_{0.05}MA_{0.1}FA_{0.85}PbI_3$|3F-PEA|ETL|Ag	1.15	23.9	[83]
	Iso-butylamine bromide (i-BABr)	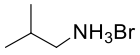	*In-situ* growth (solvent:IPA)	80% of initial PCE, 500 h, 85 °C, 15 ± 5%RH (unencapsulated)	ITO|SnO_2|$FA_{0.83}Cs_{0.17}PbI_3$ |i-BABr|Spiro-OMeTAD|Au	1.18 (15.35)	23.4 (19.5)	[84]
	Oleylammonium iodide (OLAI)	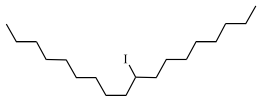	*In-situ* growth (solvent:chloroform)	95% of initial PCE, damp-heat test (IEC 61 215:2016) (encapsulated)	ITO|2PACz|$FA_{0.7}MA_{0.3}PbI_3$ |OLAI|C60:BCP|Ag	1.20	24.3	[85]
	Octylammonium iodide (OAI)	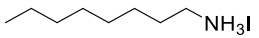	*In-situ* growth (solvent:IPA)	87% of initial PCE, 1000 h, 25 °C, 25%RH (unencapsulated)	FTO|paa-QD-SnO_2@ c-TiO_2|$FAPbI_3$|OAI| Spiro-OMeTAD|Au	1.18 (12.10)	25.4 (21.7)	[49]
3D/1D	Propargylammonium iodide (PAI)	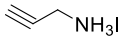	*In-situ* growth (solvent:IPA)	93% of initial PCE, 3055 h, 1 sun, N_2 (unencapsulated)	ITO|SnO_2|$Cs_{0.08}FA_{0.66}MA_{0.26}PbI_{2.74}Br_{0.1}Cl_{0.16}$|PAI| Spiro-OMeTAD|Au	1.11	21.2	[79]
	Benzimidazole iodide (BnI)	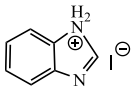	*In-situ* growth (solvent:DMF: DMSO=95:5v/v)	95.3% of initial PCE, 3072 h, 1 sun, N_2	ITO|PTAA|$Cs_{0.05}FA_{0.81}MA_{0.14}PbI_{2.55}Br_{0.45}$|BnI|C60:BCP|Ag	1.13	21.2	[86]

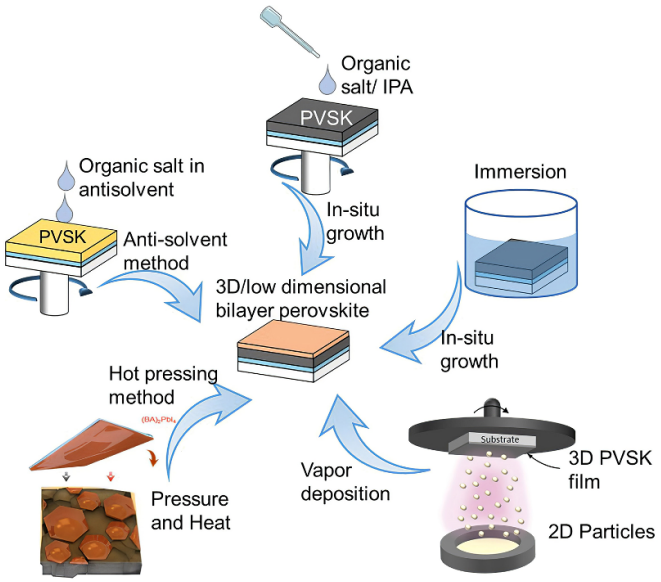

Figure 2. Schematic diagram of deposition methods for 3D/low-dimensional bilayer perovskite, including *in situ* growth method, anti-solvent method, solvent-free method (vapor deposition and hot-pressing method). PVSK is referred to perovskite.

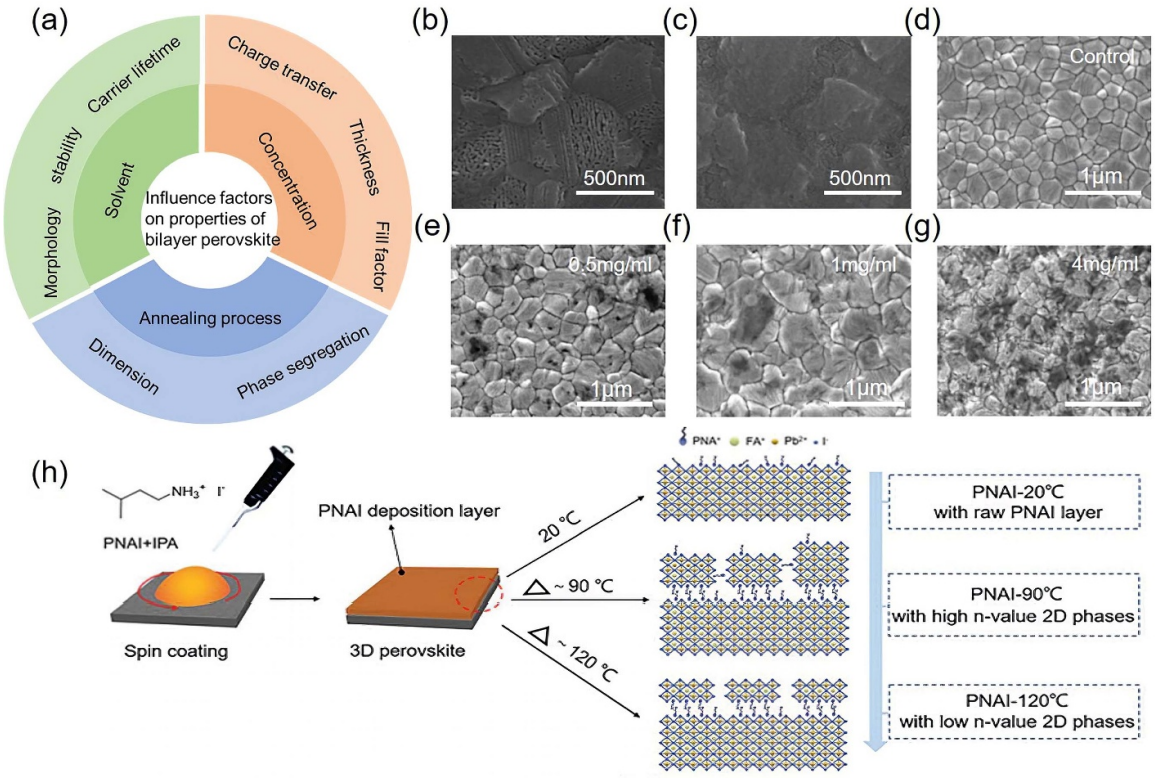

Figure 3. (a) The influence of the deposition method of low-dimensional perovskite to the properties of bilayer perovskite. Top-view SEM images of the perovskite film after depositing ammonium salt solution with different solvent: (b) IPA, and (c) chloroform. Reproduced from [27]. CC BY 3.0. Top-view SEM images of perovskite films after depositing ammonium salt solution with different concentrations: (d) 0, (e) 0.5, (f) 1, and (g) 4 mg ml^{-1}. [87] John Wiley & Sons. [© 2019 WILEY-VCH Verlag GmbH & Co. KGaA, Weinheim]. (h) Schematic illustration of the influence of annealing temperature to the 2D perovskite layer formation. Reproduced from [88] with permission from the Royal Society of Chemistry.

2.3. Other methods

There are also many other methods have been used to construct 3D/2D bilayer perovskite film. Zhao *et al* achieved a 3D/2D vertical hetero-structure by physically stacking pre-synthesized $(BA)_4AgBiBr_8$ nanosheets onto $FAPbI_3$ perovskites through van der Waals integration strategy. The $(BA)_4AgBiBr_8$ has a large bandgap and form type I

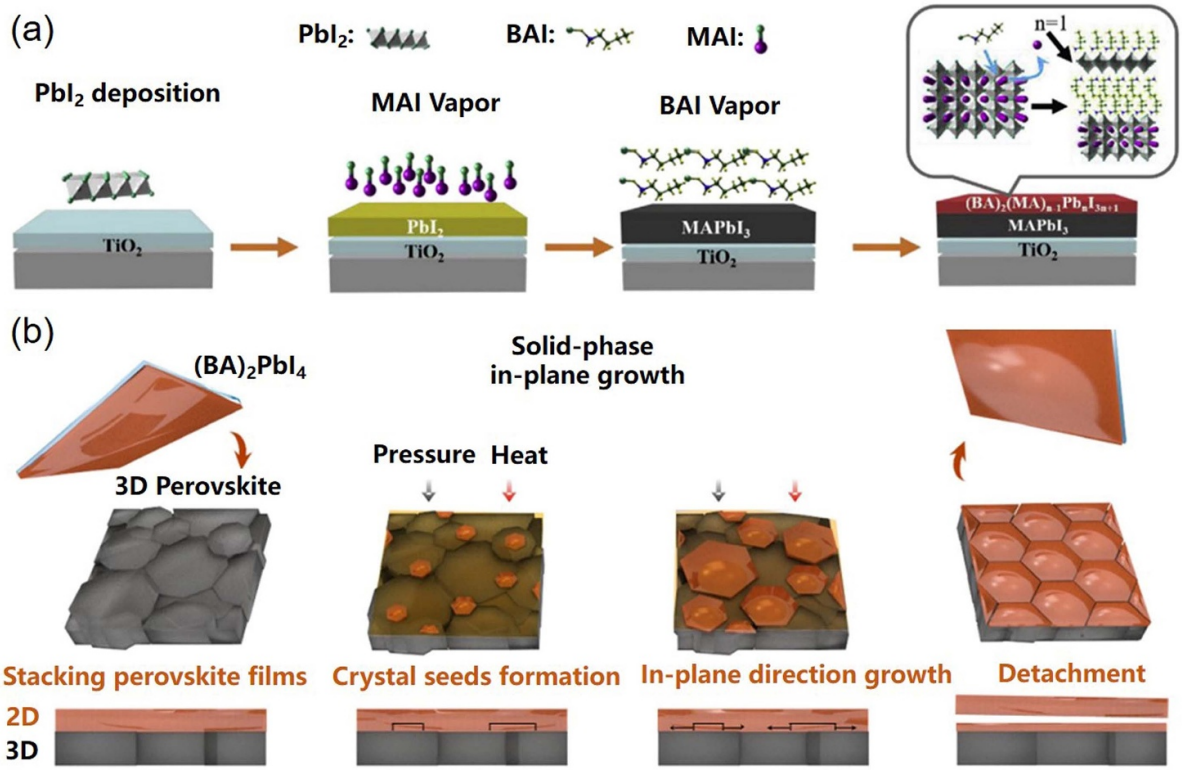

Figure 4. (a) Growth diagram of vapor deposition of 3D/2D perovskite film. The n value represents the number of perovskite layers between the two BA molecules. Reprinted from [95], Copyright (2019), with permission from Elsevier. (b) Top view and sectional sketch of $(BA)_2PbI_4$ film fabricated on 3D perovskite substrate by solid-phase in-plane method. In a cross section of a perovskite layer, black dotted lines and black arrows indicate the formation of crystal seeds and the growth of in-plane grains, respectively. Reproduced from [97], with permission from Springer Nature.

heterojunction with the $FAPbI_3$ perovskite, which can inhibit the interface trap-assisted recombination and effectively slow down the diffusion of iodide from perovskite to metal electrode. As a result, a PCE of 24.5% was achieved with an improved V_{OC} from 1.13 V to 1.17 V [98]. Zheng *et al* developed a spontaneous interfacial manipulation strategy to manufacture 3D/2D bilayer perovskite. During the annealing process, the larger size GA^+ is pushed out from the 3D $CsPbI_xBr_{1-x}$ perovskite crystals and react with the unsaturated Pb^{2+} at the surface of the film, forming an ultrathin GA_2PbI_4 2D layer on the surface of the 3D film [99]. Xu *et al* developed an aerosol-liquid-solid process to produce high-quality, thick 3D/2D bilayer perovskite films for x-ray detectors. Firstly, PEAI, MAI and PbI_2 were mixed in N,N-dimethylformamide (DMF)/dimethyl sulfoxide (DMSO) to form 2D perovskite precursor solution, while MAI and PbI_2 were mixed in DMF/DMSO to form the precursor solution of $MAPbI_3$. Aerosol droplets of 2D perovskite are first generated by their precursor solution under an ultrasonic atomizer and then transported to the nozzle by nitrogen. When these droplets reach the preheated fluorinated-doped SnO_2 (FTO) glass at 140 °C, 2D perovskite forms immediately due to equilibrium solvent volatilization and perovskite crystallization. Then, the $MAPbI_3$ film with 60 μm thickness was deposited on the 2D layer by another aerosol-liquid-solid process, resulting of bilayer structure [100].

2.4. Deposition bilayer perovskite with larger size

By virtue of the advantages in making high efficiency and stability small area solar cell with bilayer perovskite, researchers applied this strategy for making large area solar modules. Liu *et al* prepared 3D/2D bilayer perovskite based modules with an active area of 26 cm^2 by spin-coating method. Their champion efficiency was 21.4% and a continuous operational stability more than 1100 h was achieved [101]. However, spin-coating method is generally limited to a scale of 10 cm × 10 cm and a large of portion of the precursor ink is wasted in the process. Therefore, a successful integration of scalable coating strategies may not only improve the photovoltaic performance, but also meet the needs of industrial production.

The methods of fabricating perovskite film on a large size substrate can be categorized to wet printing and dry vacuum deposition as well, which have been well reviewed by previous reports [47, 102]. Briefly, wet printing method including blade or bar coating, slot-die coating, inkjet printing (IJP) and spray coating (figures 5(a)–(c)). For blade coating, the ink is directly loaded onto the substrate and a blade is used to spread the ink over the substrate. Therefore, the film thickness is mainly dependent on the meniscus that formed between the blade and the substrate. The meniscus can be controlled by the geometry of the blade, the gap between the blade and the

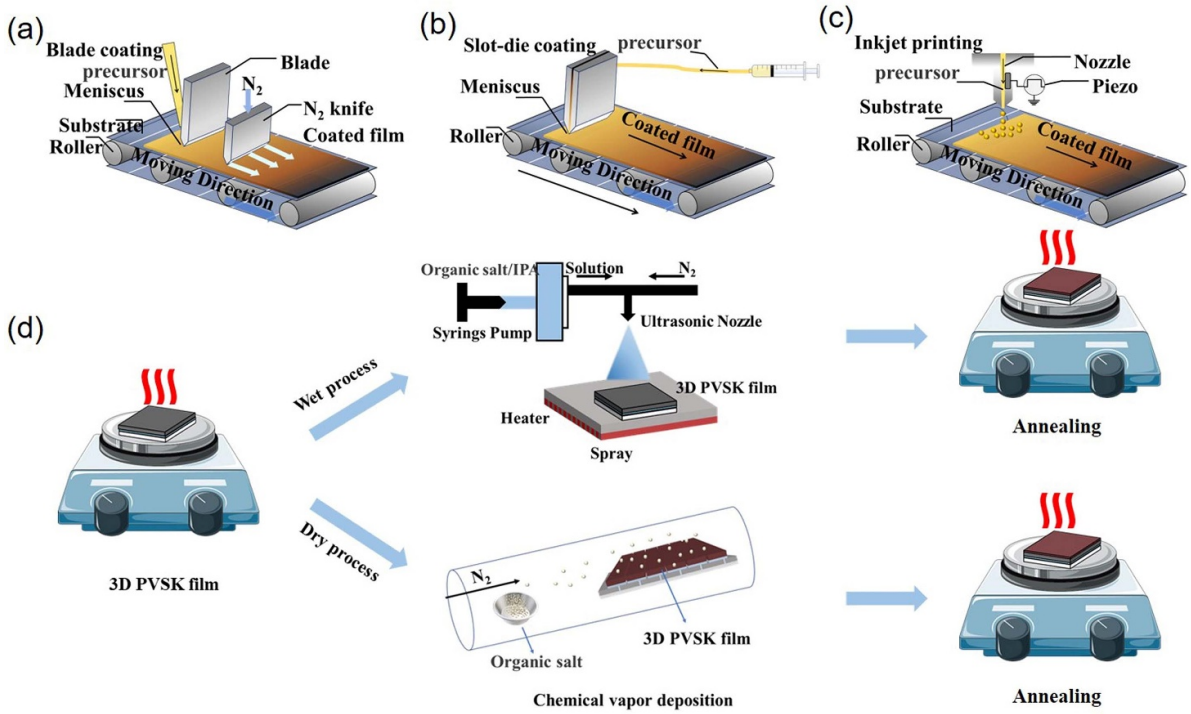

Figure 5. Schematic diagram of 3D perovskite film preparation: (a) blade coating, (b) slot-die coating, (c) inkjet printing. Reproduced from [102]. CC BY 4.0. (d) Proposed schematic diagram of large area low-dimensional perovskite film deposition: spraying and chemical vacuum deposition. PVSK is referred to perovskite.

substrate, the speed of the blade relative to the substrate, the viscosity of the ink, and the wettability of the substrate [103]. Slot-die coating uses an ink reservoir in coating head with a thin slit to apply ink over the substrate. The deposition process involves transporting the ink from the coating head to the substrate, forming a continuous liquid meniscus between the lips of the heads and substrate. The liquid meniscus of the ink moves onto the solution film on the matrix. Therefore, beyond the advantages mentioned in the blade-coating method, the slot-die coating method can be pre-metered to obtain uniform films and dapted for continuous fabrication. In addition, the quality of perovskite films can be modified by the temperature of the substrate and blowing gas, which control the crystal growth process [104]. IJP works in a similar way to the inkjet system of office printers. It uses the muzzle of a gun to drop the ink from a piezo-driven inkjet head. Considering the dispersion of ink droplets on the substrate during ink printing, the use of anti-solvent is not suitable for this process [105]. Spray coating is a common solution deposition technique. Ultrasonic vibration is used to create ink droplets under the tension of kHZ, while compressed gas is used to spray the ink droplet onto the substrate. These droplets then stick to the substrate to form a continuous wet film, which is dried to form a uniform film [106]. Vapor deposition is a mature deposition technology in the thin-film photovoltaic filed, such as CdTe or Cu(In,Ga)Se_2 (CIGS) based solar cell. There are a number of reports that use chemical vapor deposition (CVD), thermal-vapor deposition, low vacuum single step processing [107], sequential vapor deposition processing [108], and growth at atmospheric conditions [109] to fabricate large area perovskite film, showing promising results.

Bu *et al* prepared a 3D/2D bilayer perovskite by combining slot-die coating and spin-coating, achieving champion efficiencies of 20.4% and 19.5% for PSMs with active areas of 17.1 and 65.0 cm^2, respectively [84]. On the other hand, Zendehdel *et al* first spin-coated the 3D perovskite film, followed which the 2D perovskite was deposited by blade coating with a blade speed of 0.1 mm S^{-1}. The films showed a high uniformity and reproducibility morphology, in addition to nearly zero waste of 2D precursor ink. PCE of 18.8% was achieved for the PSMs with an active area of more than 10.0 cm^2 [110].

When fabricating larger area bilayer perovskite film with scalable techniques, the 3D layer can be readily prepared by the above methods, while the low-dimensional perovskite layer can be sequentially deposited by spraying or evaporating the ammonium salt on the 3D layer, followed by a post-annealing process (the proposed process is shown in figure 5(d)). In addition, it can also be deposited by immersing the 3D layer into a solution containing specific ammonium salts. The one we need to pay attention is that there is inherent difference in the formation process between 3D and low-dimensional perovskite layers. When depositing the 3D perovskite layer, all components, such as AX and BX_2 that used to construct the final ABX_3 film are in the precursor. On the other hand, only ammonium salts, i.e. AX is in the precursor for low-dimensional perovskite, while the other component, BX_2 is on the surface of the substrate, i.e. the 3D perovskite

layer. Therefore, we can divide the deposition process of low-dimensional perovskite into three steps, such as spreading, drying, and post-annealing, in which the spreading can be easily conducted by printing techniques.

3. Beneficial effects of bilayer structure

As summarized in figure 6, the main factors which causes the decomposition of perovskite films are moisture, thermal stress, oxygen, and UV light illumination. Compared to 3D perovskite structures, low-dimensional perovskite not only exhibits its better resistance to the above stimuli, but also features a lower ion diffusion coefficient.

3.1. Enhance the moisture stability

In a 3D/2D bilayer perovskite film, the hydrophobic long chain cation in 2D perovskite is expected to be exposed to the environment, thus protecting the vulnerable 3D layer from the invasion of moisture or oxygen. The surface free energy of 3D/2D bilayer perovskite was significantly reduced compared to the original 3D perovskite film [111]. As shown in figure 7(a), Cheng *et al* reported four representative ammonium salts featuring different chain lengths to build 3D/2D bilayer perovskite films, i.e. phenylmethylammonium iodide (PMAI), PEAI, phenylpropylammonium iodide (PPAI), and phenylbutylammonium iodide (PBAI). The contact angle of the films increases along with the increased length of the alkyl chain (figure 7(b)) [112]. The decomposition of the beneath 3D perovskite film to PbI_2 upon exposure to moisture is effectively slowed down (figure 7(c)). As a result, the devices based on 3D/PPAI-2D bilayer perovskite showed obvious improved moisture stability than the 3D perovskite when aged at high humidity environment (RH $= 85 \pm 5\%$) (figure 7(d)) [112]. Pham *et al* report a method for *in-situ* generation of 1D lead pyrrole iodide (1D $PyPbI_3$) at the top of 3D perovskite $MAPbI_3$. The un-encapsulated 3D/1D devices maintained an initial efficiency of 97.5%, while it is 86.7% for the 3D devices under RH% between 30 and 65% [113].

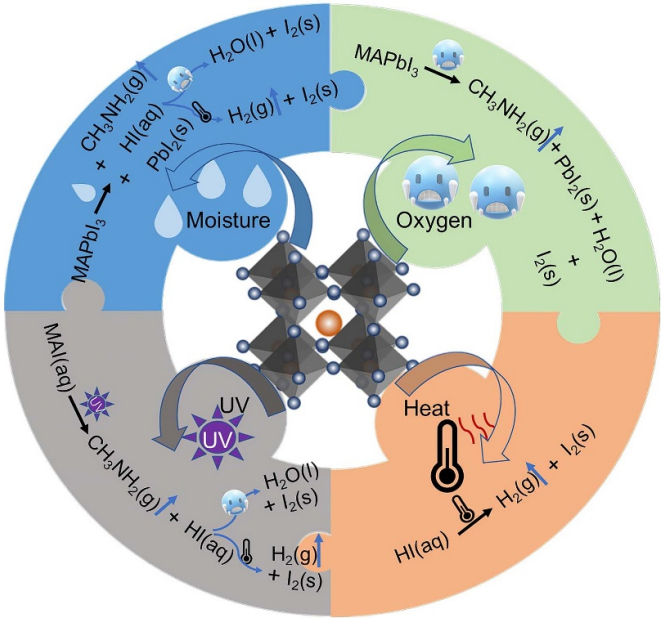

Figure 6. A summary of possible degradation mechanism of $MAPbI_3$ perovskite films under moisture, oxygen, UV light, and thermal stress.

3.2. Improved thermal stability

Thermal stress is another factor leading to the degradation of perovskite films. As reported by Kim *et al*, $MAPbI_3$ perovskite decomposes to CH_3I, NH_3 and PbI_2 at high temperature (>80 °C). In addition, the crystal structure and lattice parameters of perovskite may also change at elevated temperature, resulting of an evolution of light harvesting ability, charge transfer properties, and thus the device performance [114].

It is interesting to note many reports demonstrated that instead of decomposition, the morphology and charge extraction properties of 3D/2D perovskite can be improved after thermal aging. Sutanto *et al* monitored the crystal structure and the interface evolution in 3D and 3D/2D perovskite, i.e. 3D and 3D/2-TMA-2D perovskite (2-TMAI refers to 2-thiophenemethylammonium iodide) in the thermal cycling by *in-situ* x-ray scattering (figures 8(a) and (b)) [115]. As shown in the figures 8(c) and (d), 3D perovskite film degrades after thermal cycling, with a XRD diffraction peak intensity decrease of 15%, while the 3D/2D film is more robust under the same condition. Moreover, in the case of 3D/2-TMA-2D, the peak intensity of $n = 1$ and $n = 2$ gradually decreases in the thermal aging process and a new peak emerges, indicating the formation of a mixed intermediate structure at the interface. And they also concluded that the molecular structure of ammonium salt in the 3D/2D perovskite is important (figures 8(e) and (f)). Azmi *et al* prepared damp-heat stable PSCs by tailoring the dimensional fragments of 2D perovskite layers, in which oleylammonium iodide was used to form the 2D layer. The inverted PSCs obtained PCE of 24.3% and retain 95% of the initial performance after 1000 h damp-heat test conditions [85].

3.3. Improved illumination stability

Encapsulation is an efficient strategy to protect the degradation of perovskite film from humidity, oxygen etc, and even the decomposition reaction under thermal stress can be mitigated. However, many studies show a decomposition of perovskite film under continuous illumination, which could be an intrinsic disadvantage of metal halide perovskite materials and the corresponding devices. The defects are reported to be one of the main reasons for the degradation caused by light exposure [116]. Low-dimensional perovskite can passivate defects on the surface and grain boundaries, thus preventing the degradation of 3D perovskite under illumination. Compared to 3D/2D perovskite, highly conductive 1D perovskite can alleviate lattice mismatch in 3D/1D films, passivate interface defects, and improve stability without sacrificing efficiency of devices [117]. Yang *et al* introduced a

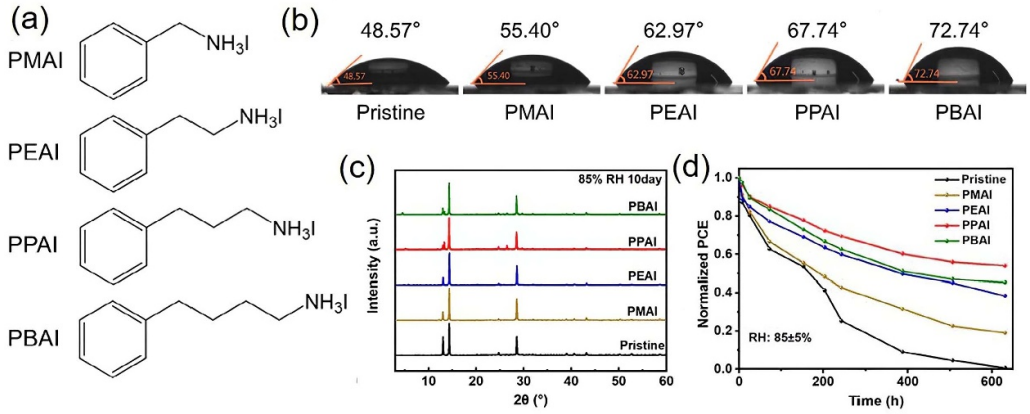

Figure 7. (a) Molecular structure of four ammonium salts feature with different chain lengths. (b) Water contact angle of 3D/2D bilayer perovskite films. (c) XRD patterns of 3D/2D bilayer perovskite films when stored at 85% RH for 10 d. (d) PCE changes of PSCs based on 3D/2D bilayer perovskite films when placed at 85 ± 5% RH for 600 h. [112] John Wiley & Sons. [© 2021 Wiley-VCH GmbH].

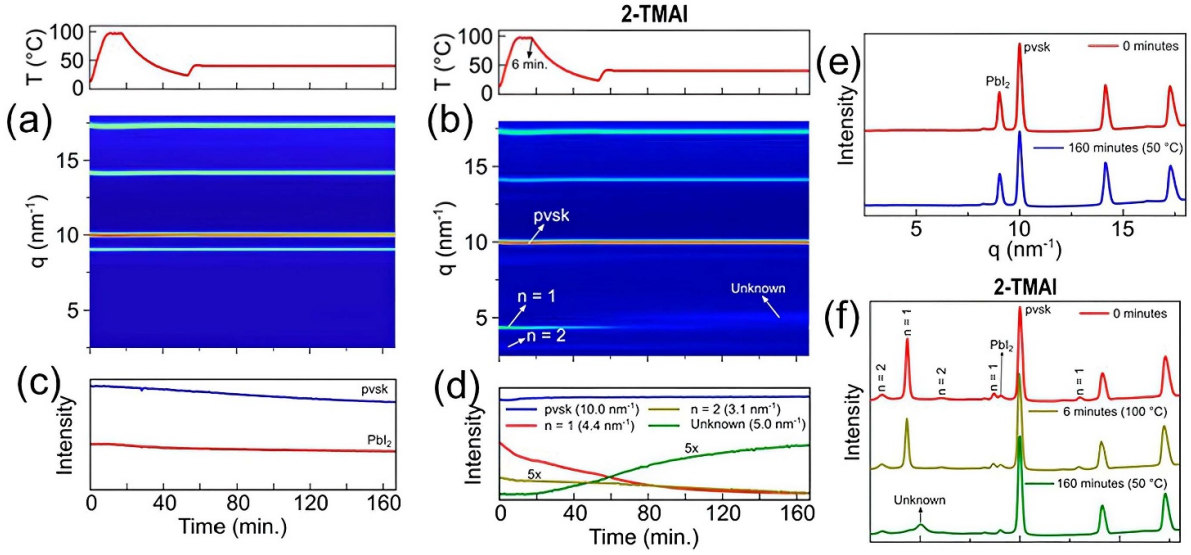

Figure 8. The *in-situ* GIWAXS diffraction as a function of time and temperature for (a) 3D, and (b) 3D/2-TMA-2D bilayer perovskite films. The variation of the intensity of each main peak with time for (c) 3D, and (d) 3D/2-TMA-2D bilayer perovskite films. XRD diffraction patterns at different times for (e) 3D, and (f) 3D/2-TMA-2D bilayer perovskite films. Reproduced from [115]. CC BY 4.0.

polymerizable propargylammonium (PA^+) polymer to cross-link with 3D perovskite films form 3D/1D perovskite heterostructure. The corresponding device achieved a champion efficiency of 21.2% with an impressive stability. It remained 93% of the initial efficiency after 3055 h continuous operation [79].

3.4. Suppressed ion migration

In addition to environmental stimuli, perovskite materials are reported to be unstable due to the internal ion migration. Due to the low activation energy (i.e. 0.5–0.8 eV for MA^+, and 0.2–0.7 eV for I^-), halogen ions migrate easily under the activation of light, heat, or bias, which lead to iodide-rich and bromide-rich domains, i.e. phase segregation as well as lattice point defects [118]. These migrated ions cause irreversible damage to the active layers and even the metal electrode. In addition, phase segregation can significantly change the optoelectronic properties such as the bandgap and energy alignment of perovskite films [119, 120].

The origin of ion migration in perovskites is demonstrated to be associate to the defect states. Since the grain boundary has a much higher defect density than the bulk region [121], it is generally believed that grain boundary is the main migration channel [122]. Passivation of the grain boundary with low-dimensional perovskite reduces the defect density and slows down ion migration, thus improving the stability of the device to a certain extent. In order to explain the mechanism of ion migration, the value of E_a has been used to quantify the tendency of ion migration within a film, which can be fitted by the Nernst–Einstein equation as follows:

$$\sigma(T) = \frac{\sigma_0}{T}\exp\left(-\frac{E_a}{K_B T}\right) \quad (2)$$

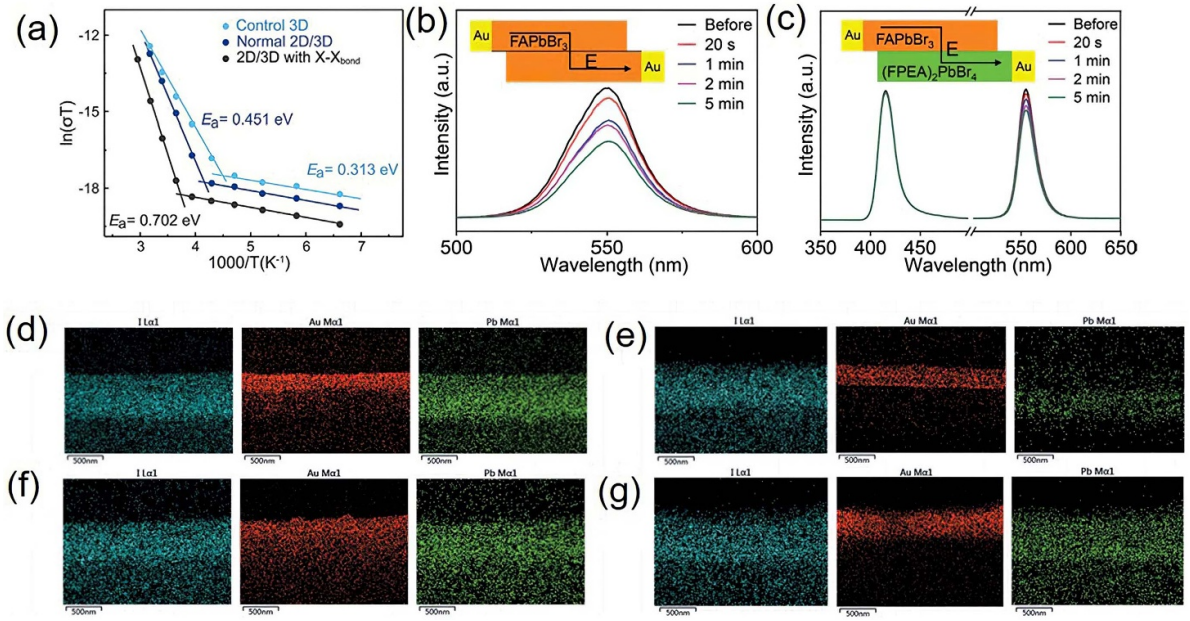

Figure 9. (a) Temperature dependent conductivity measurement for E_a extraction. Reprinted from [123], Copyright (2021), with permission from Elsevier. The PL spectra under a bias of 1 V m^{-1} for different duration: (b) 3D/3D film; (c) 3D/2D film. [124] John Wiley & Sons. [© 2021 Wiley-VCH GmbH]. Cross-section EDS profiles of I, Au, and Pb elements in fresh devices: (d) without PMAI and (e) with PMAI modifier; and in aged devices: (f) without PMAI, and (g) with PMAI layer. Scalebar: 500 nm. Reproduced from [125] with permission from the Royal Society of Chemistry.

where the slope of the $\ln(\sigma)^{-1}/kT$ relation denotes the E_a Value. Fu *et al* extracted E_a by measuring the conductivity of perovskite film at different temperatures. They introduced a concept of halogen-halogen bonding to immobilize the halide anions located on grain boundary. 2-(2,3,5,6-tetrafluoro-4-iodophenoxy)ethan-1-ammonium was used as the 2D precursor to construct of 3D/2D bilayer film. The E_a is significantly increased from 0.313 to 0.702 eV at the transition temperature of 250 K. As a result, the migration of ions slows down (figure 9(a)) [123].

He *et al* studied the PL behavior of perovskite films based on 3D/3D and 3D/2D structure under a poling electric field (figures 9(b) and (c)). In 3D/2D films, the PL intensity of the 2D perovskite is robust and the 3D perovskite remains more than 80% of its initial intensity. In contrast, the PL intensity of 3D/3D perovskite films decreases more seriously. This result suggest the ion migration is suppressed in the 3D/2D bilayer perovskite films [124]. Not only the halogen ions in perovskite, but also the migration of metal atoms/ions in the counter electrode can be inhibited by the 2D capping layer. Ye *et al* reported that the ion migration activation energy of perovskite film increased from 0.496 to 0.514 eV after the deposition of a PMAI based 2D layer [125]. Moreover, cross-section energy dispersive spectroscopy (EDS) diagrams demonstrated that PMAI effectively inhibited the migration of Au^+ from contact electrode to perovskite layer (figures 9(d)–(g)).

3.5. Morphology optimization

Previous studies have shown that the morphology, such as surface morphology, roughness, and grain size changes after the deposition of the 2D layer [127]. Lv *et al* studied the morphology of the 3D/2D bilayer perovskite film, in which the 2D layer is based on PEAI and $PEAI_xBr_{1-x}$ [127]. A thin and dense capping layer emerged on the 3D perovskite layer, which is the PEA-based 2D layer (figure 10(a)). Moreover, new phase with flake-shape emerged as demonstrated by top-view SEM image (figure 10(b)) and atomic force microscope (AFM) images (figure 10(c)) [126]. Elsenety *et al* deposited a layer of 1D $(CH_3)_3SPbI_3$ perovskite on the surface of 3D (FA/MA/Cs)$PbI_{3-x}Br_x$ perovskite. 1D perovskite was mainly located in the valley of the grain boundary, which made the surface smoother by reducing the height difference [128]. Notably, this morphology facilitates the extraction of carriers while inhibits ion migration, which are essential for efficient and stable PSCs.

3.6. Defect passivation

As discussed in previous sections, it is important to take steps to passivate defects. The defects may generate following three different scenarios: (a) surface defects; (b) grain boundaries; (c) point defects when halogens escape during annealing [129]. For example, during the crystallization of 3D perovskite, uncoordinated PbI_2 will form when the surrounding cation, such as MA^+/FA^+ is insufficient [130]. These PbI_2 with poor electronic properties potentially act as the recombination centers that capture free charge, leading to severe non-radiative recombination. By depositing a delicate designed ammonium salt, the defects can be reduced reacting with PbI_2 to form 2D perovskite. In addition, it is reported that halide, such as Br^- tend to escape from the mixed halide perovskites,

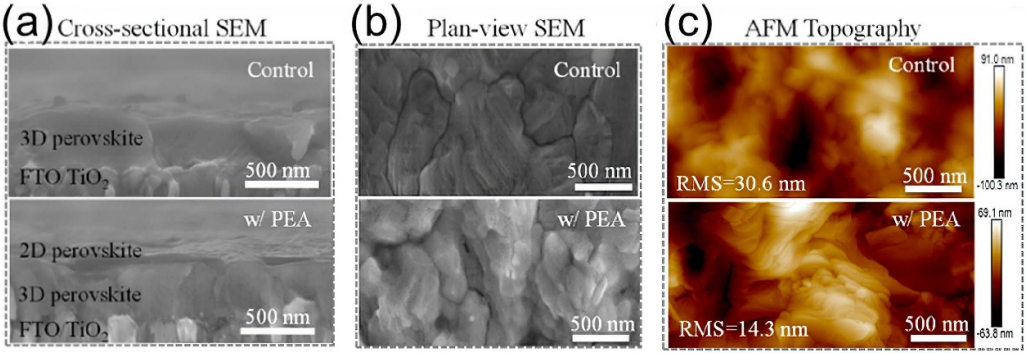

Figure 10. The morphology study of perovskite covered w/o PEA-based 2D layer: (a) cross-sectional, (b) top-view SEM images, and (c) AFM images. Reprinted with permission from [126]. Copyright (2019) American Chemical Society.

thus generates point defects [131]. These halide vacancies can be supplemented during the deposition of the 2D layer [132].

4. 3D/2D bilayer perovskite for large area modules

4.1. Efficiency

Despite the world-record efficiency of PSCs is comparable to crystalline silicon solar cells (25.7 vs. 26.7%) and higher than other thin-film solar cells such as CIGS and CdTe, the cell-to-module efficiency gap is more significant for perovskite photovoltaic than other technologies [133, 134]. For larger area modules (>10 000 cm^2), the record efficiencies for Si, CIGS, and CdTe are 24.4%, 18.6%, and 19.0%, respectively, while it is only 17.9% for PSCs with a much smaller active area of ∼1000 cm^2 [135]. Therefore, it is urgent to fabricate large area PSMs with high efficiency.

In comparison with other PV technologies, it is not practical to manufacture a single PSC on a large substrate because of the considerable loss of parasitic resistance in transparent conducting electrodes over long distances. Additional scribing steps are needed to divide large area devices into small areas sub-cells and form electrical connections between these sub-cells [136]. Therefore, series or parallel design are commonly used to interconnect these sub-cells, which generates additional losses, in the form of dead region losses and interconnect resistance losses (figure 11(a)) [137]. To date, most of the efficient perovskite modules (PCE > 18%) are based on series-interconnection design. Recently, Yang *et al* designed a parallel-interconnected module structure, in which silver grids were deposited under the perovskite to minimize the series resistance of FTO substrate and act as a current collector (figure 11(b)). They achieved a certified quasi-stabilized efficiency of 16.6% with an active area of 20.77 cm^2 [80]. Beyond these disadvantages, the PCE of modules also decreases due to an increase of inhomogeneity in the active layers.

To minimize the dead area and improve the geometric fill factors, which is the ratio of the photoactive area to the total area. Moon *et al* reported that the total loss as a function of the active zone widths (W_a) with various dead zone widths (W_d). At a fixed W_a of about 6 mm, the total loss decreases from 35% to 10% when reduce the W_d from 3 to 0.5 mm (figure 11(c)) [139]. As shown in figure 11(d), Wilkinson *et al* studied three different unit designs in turn: design A: (a cell with no metal grid), design B: (a cell with the metal grid consisting of parallel metal bus-bars), design C: (a cell with the metal grid consisting of parallel bus-bars and fingers). The PCE value is higher for the design C when the area is >200 cm^2. This finding suggests that the design of metal grids in transparent conducting oxide (TCO) is important to improve the PCE values of large-area modules [140].

Identification and controlling the inhomogeneity of active layers, such as perovskite, charge transporting layers on a large size substrate is another challenge. Rakocevic *et al* proposed five efficient techniques to analyzed the inhomogeneity of layers in PSMs, i.e. electroluminescence (EL), dark lock-in thermography (DLIT), multi-wavelength light-beam induced current and microscopic PL spectroscopy (μPLS). Also, the inhomogeneity has been categorized to five types according to the inhomogeneity size and the characterization method used to localize them (table 2 and figure 12(a)). EDX analysis suggests that inhomogeneity of type 1 is micrometer-sized organic carbon-based particles (see DLIT image in figure 12(b)), which is presumed to be associated with the phenyl-C61-butyric acid methyl ester (PCBM) from electron transporting layer. Type 2 is larger than type 1 (300 vs. 10 μm) and mainly located at the interconnections of sub-cells. It is caused by the accumulation of conductive particles at P1 or metals at P3 isolation lines. For example, SEM images identified the Au cluster at the P3 interconnection (figure 12(c)). The size of type 3 is up to 500 μm and possibly originated from the non-optimized colloidal precursor solution and process cleanliness (figure 12(d)). As summarized in table 2, inhomogeneity of type 5 represent millimeter-sized areas that can span across multiple cells in a module. To obtain modules with both high efficiency and stability, all types of inhomogeneity should be eliminated.

3D/2D bilayer structure has been demonstrated to be beneficial for the homogeneity of the large-area perovskite films. Kim *et al* introduced 1-decyl-3-methylimidazolium bromide (DMIMB) on the surface of 3D perovskite to form a uniform 2D layer. The 3D/2D sample has a higher work function (5.07 vs. 4.84 eV) and more uniform localized

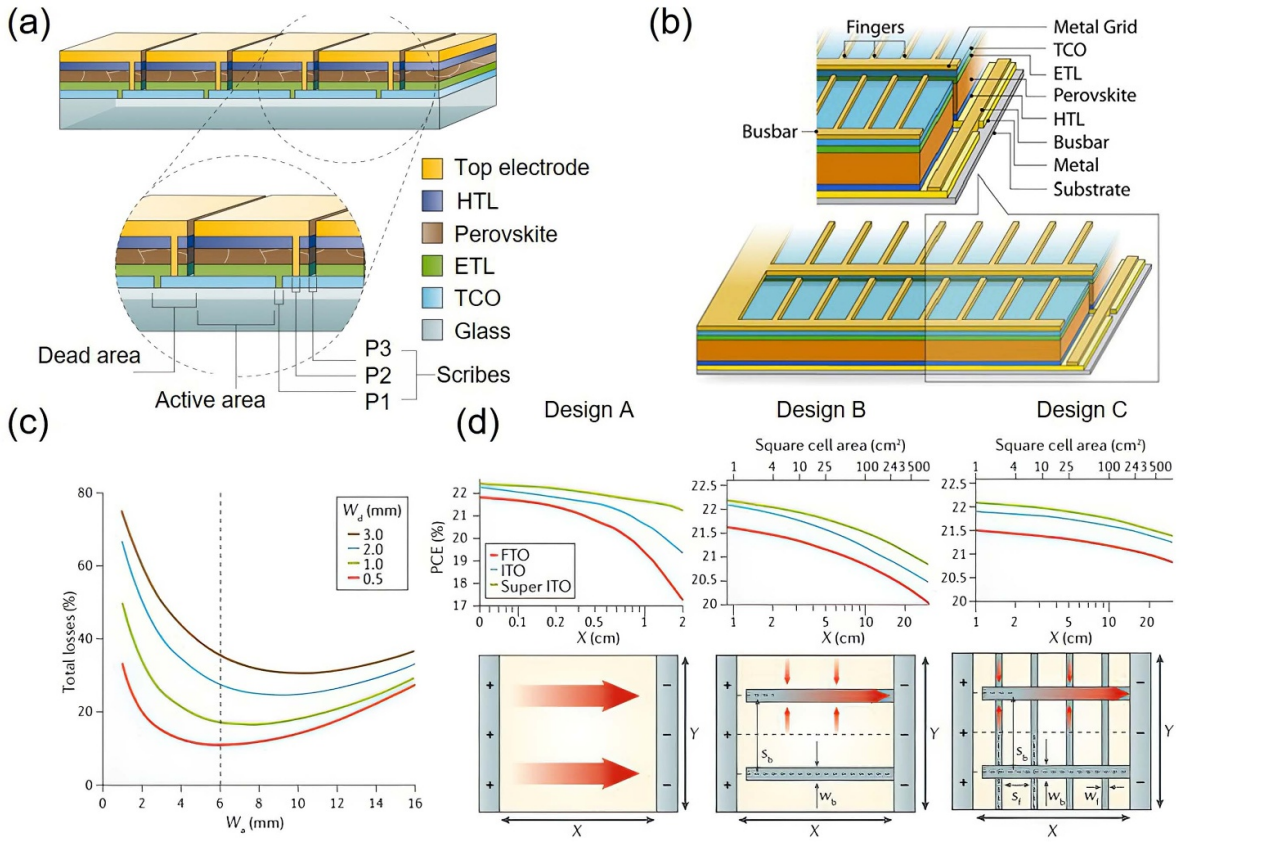

Figure 11. Schematic diagram of perovskite module design: (a) series-interconnection. Reproduced from [136], with permission from Springer Nature and (b) parallel-interconnection. Reprinted from [138], Copyright (2018), with permission from Elsevier. (c) The impact of the module-scribing geometry on the total power loss in a perovskite module. The plot shows the total losses as a function of the active-area width (W_a) for various dead-area widths (W_d). (d) Plots (top) showing that the PCEs as a function of cell width (X) between the electrodes and the square cell area. Three cell designs were modelled (bottom): A (a cell without a metal grid), B (a cell with a metal grid consisting of parallel metal bus bars) and C (a cell with a metal grid consisting of parallel metal bus bars and fingers). Reproduced from [136], with permission from Springer Nature.

Table 2. The classification of identified inhomogeneity into five types. [141] John Wiley & Sons. [© 2019 WILEY-VCH Verlag GmbH & Co. KGaA, Weinheim].

	Type 1	Type 2	Type 3	Type 4	Type 5
Characterization method	DLIT and local maps μPLS	DLIT	EL and μPLS	EL and μPLS	EL and μPLS
Size	30 μm or less	up to 300 μm	Up to 500 μm	Full cell	Millimeter-sized areas
Source	Unfiltered PCBM solution and lack of process cleanliness	Conductive particles in P1 or P3 compromising isolation	Nonoptimized colloidal precursor solution and process cleanliness	Presumed to be due to interconnection defects	Differences in nonradiative recombination due to perovskite/PCBM/TiO_2 interface
Effect on performance	Can cause full cell damage during short-term performance	Decrease in FF or inactive cells due to dysfunctional interconnections	Decrease in J_{SC} and V_{OC} performance and possible effect on long-term stability	Inactive cells causing lower V_{OC} in modules	Lower J_{SC} due to current mismatch among cells in a module
Loss decrease strategy	Filter solutions and assure controlled process atmosphere for all steps	Laser patterning with particle suction system	Precursor solution engineering and optimization of deposition method for controlled crystallization	Optimized patterning method using laser ablation	Optimize deposition method (precursor deposition, solvent evaporation, drying) for perovskite homogeneity

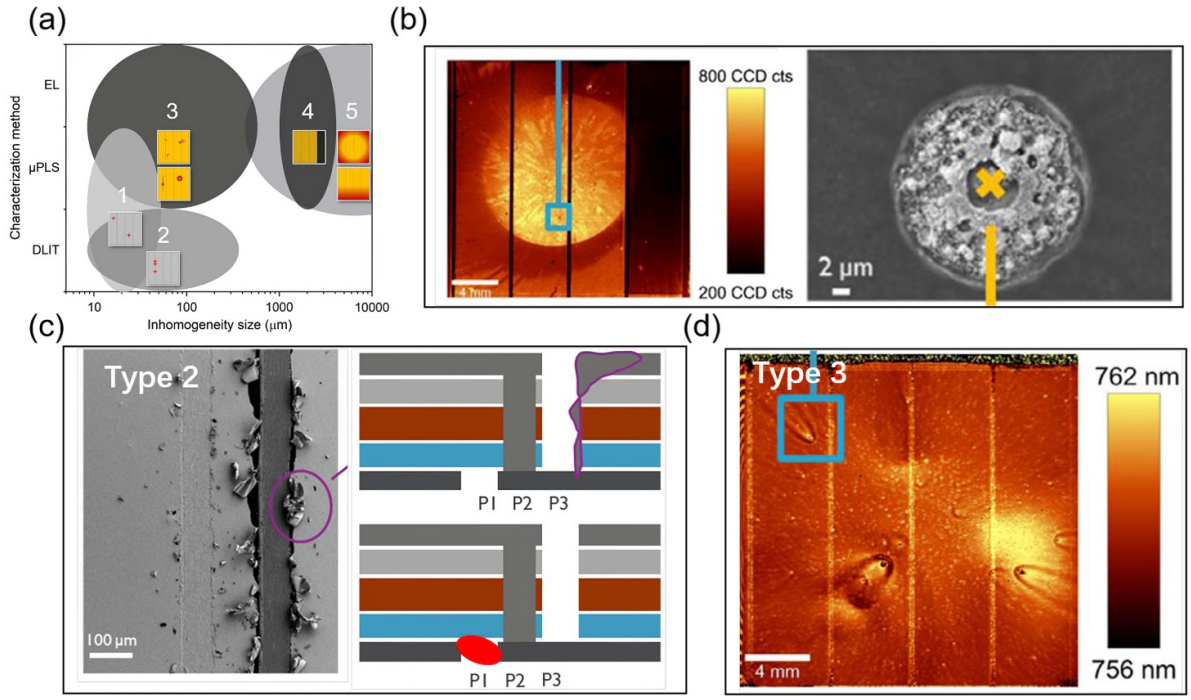

Figure 12. (a) Five types of inhomogeneity in perovskite modules categorized by the size and imaging method used to detect them. (b) DLIT and SEM secondary electron image of type 1 inhomogeneity. (c) SEM image of mechanically patterned interconnections indicating accumulation of Au material at the P3 interconnection. On the right is a schematic of a short circuit caused by conductive particles accumulate at P1 or metals at P3 isolation lines. (d) DLIT image of type 3 inhomogeneity. [141] John Wiley & Sons. [© 2019 WILEY-VCH Verlag GmbH & Co. KGaA, Weinheim].

nanoscale surface area due to 2D layer formation. As a result, a champion PCE of 18.4% was achieved with an active area of 22.6 cm^2 [142].

4.2. Stability

Generally, cost, efficiency and stability are the golden triangle to evaluate the technical feasibility of PV technologies for commercialization. As calculated by Cheng and Ding, PSCs show great potential to be a low-cost PV technology compared to their counterparts once the lifetime increases to 25 years. However, the longest lifetime of PSCs under continuous operation is ∼10 000 h, which is far behind the 25 year lifetime guarantee for most commercially available PV modules. Recently, the T_{90} of PSMs under continuous operation have been reported to exceed 1187 h, which is inspiring but still obviously lagging behind the small area cells. The stability of perovskite modules is more complicate than the small area cells. Firstly, the P1, P2, and P3 increase the possibility of degradation, such as the direct contact between perovskite and metal electrode after P2 processing, the exposure of perovskite to atmosphere after P3 process. Secondly, in a partially shaded module (by dirt or cloud), the shaded sub-cells are subjected to a high reverse bias, which could lead to local hot spots and inverted-bias junction damage.

By virtue of the improvement of stability in small area cells, the bilayer structure has been tried to fabricate more stable modules. For example, by introducing a trimethylphenylammonium bromide (PTABr) layer, Ma *et al* not only reduced the point defects of Br-vacancy of the 3D perovskite film, but also improved the uniformity of the larger area film. A champion efficiency of 17.0% with an active area of 10.0 cm^2 was achieved for the modules based on wide bandgap perovskite. Moreover, the modules sustained 81% of the initial efficiency after aging for 1000 h at ambient condition, while it is only 49% for the control [143]. 2D layers have also been used to block ion diffusion channels between the perovskite and metal electrode at the P2 interface. Xu *et al* simultaneously improved the efficiency and stability of PSMs by doping a Br-containing alkyl ammonium salt (TBAB) into the perovskite precursor. The efficiency of PSMs containing four sub-cells remained 89% of the initial PCE after aging at humidity of ∼45% for 1000 h, while the control modules rapidly decreased to 30% after 480 h [144]. The reasons of this improved has been summarized as: (a) the surfactant feature of TBAB reduced the surface tension of the precursor and promoted a uniform film formation. (b) The halide anion competition (I^- and Br^-) retarded the crystallization of perovskite and improved the crystallinity. (c) The surface modification by TBA^+ not only inhibited the moisture invasion but also suppressed the escape of volatile components of 3D perovskite. Xiao *et al* suppressed the inter-diffusion and reaction between perovskite and metal electrode by depositing ∼10 nm conformal diffusion barrier (CDB) after P2 scribing (figure 13(a)). For modules without CDB, Ag was detected in the perovskite film after heating the modules in a nitrogen glove box at 85 °C for 24 h. In contrast, no Ag was detected in the module with CDB. This result suggests that the CDB layer prevents the Ag diffusion through

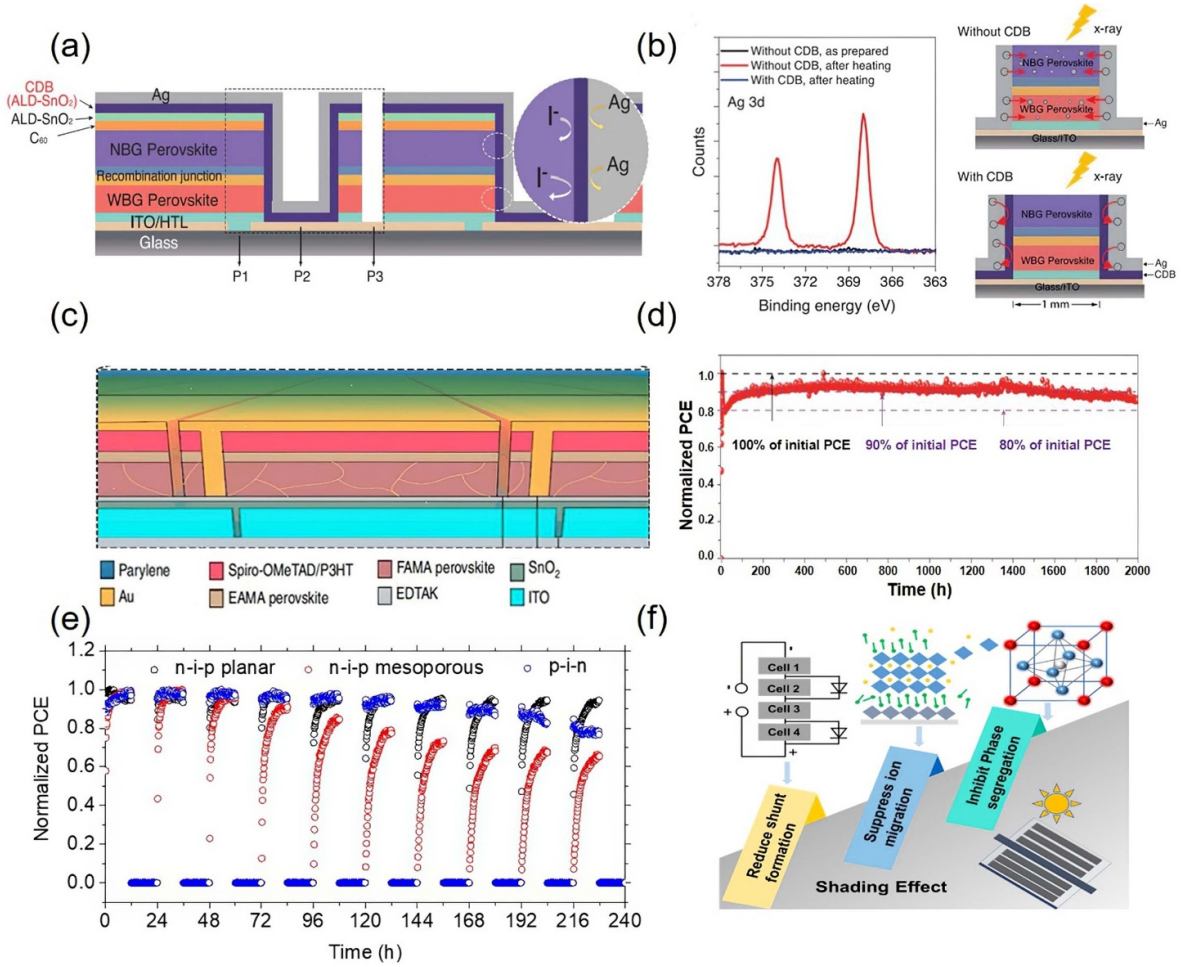

Figure 13. (a) Schematic diagram of the conformal diffusion barrier (CDB) in a series-connected all-perovskite tandem module. (b) The Ag 3*d* XPS spectra of the perovskite surface w/o CDB layer. From [145]. Reprinted with permission from AAAS. (c) Holistic interfacial treatments and encapsulations for PSMs. (d) Operational stability of a PSM after holistic interfacial treatments and encapsulation. Reproduced from [53], with permission from Springer Nature. (e) Fatigue behavior of cells with different configuration under day/night cycling aging. Reprinted from [146], Copyright (2019), with permission from Elsevier. (f) Illustration of the three strategies to limit shading effect in perovskite modules.

P2 region and improve the stability of modules (figure 13(b)) [145]. On the other hand, Yang *et al* replaced the series interconnection by parallel-interconnection to avoid direct contact between the perovskite and the metal electrode/grid. A chemically inert bismuth layer was also introduced between the BCP layer and the Ag electrode as an osmotic barrier to prevent the Ag diffusion. The module retained 97% of its initial efficiency after aging for 10 000 h under real day/night cycling [80]. In a series connected module, the hole transporting layer and perovskite are exposed to air after P3 scribed process. Liu *et al* protected the modules first with a thin layer of parylene, then fully encapsulated it by cover glass to further improve the stability (figure 13(c)). The modules maintained approximately 86% of its initial performance after 2000 h of continuous operation under AM1.5 G illumination (figure 13(d)) [53]. In addition, the structure of the perovskite devices also has a great impact on stability. Jiang *et al* found that the fatigue behavior in the day-night cycle test was due to defects in the perovskite layer caused by cyclic ions/vacancies migration and demonstrated that this fatigue behavior was strongly dependent on the charge transfer materials. Their results showed that the inverted device exhibited better fatigue stability than both planar and mesoporous-devices (figure 13(e)) [146].

In practical applications, the shading effect is a key factor that limits the lifetime of photovoltaic modules. When the sub-cells are connected in series, the shaded sub-cells block the photocurrent of the entire module, and it may be burned by bias generated by other sub-cells to resume photocurrent output [36]. Over time, these same effects may also combine with intrinsic and extrinsic ion conduction phenomena to alter component performance [106]. As illustrated by figure 13(f), beyond the use of bypass diodes, we can limit the negative effect of shading effect by suppressing the ion migration, inhibiting the phase segregation, and reducing the shunt formation within devices [147]. Deng *et al* reported a method of fast blade coating large area of perovskite films. With the help of N_2 knife, compact perovskite films were rapidly formed using volatile host solvent. They mimicked the extreme case that

one sub-cell in the module was entirely shaded, while all other sub-cells exposed to 1 sun illumination. The results show that PSMs were completely recyclable after 58 shadowing cycles, which is even better than commercial silicon and thin-film solar modules [36].

5. Outlook and perspectives

PSCs have reached a comparable efficiency with conventional PV technologies in the laboratory. The levelized cost of energy of perovskite PV is reported to be as low as *ca.* 4.0 US cents kWh^{-1} when the lifetime is 15 years, which makes it possible to play an important role in a carbon neutral society. The elongation of the lifetime, particularly for module size devices with reasonable efficiency (>20%) is the primary task for future development. Bilayer perovskite structure has been demonstrated to be efficient in increasing the stability of perovskite-based cells, but the application and optimization for module size devices are rare. We propose herein challenges and resolutions for the future development of the perovskite PV.

(a) Although this promising structure has been widely studied and reported in recent years, most of the research on bilayer perovskite is random. In order to simultaneously inherit the superior stability of low-dimensional perovskite and optoelectronic properties of 3D perovskite, new thoughts and designs are needed. By treating the 3D and low-dimensional perovskite bilayer as an 'unit', i.e. functional motif, more disruptive properties and results are expected. For example, the design of ammonium salt (for low-dimensional perovskite) and the choice of composition (for 3D perovskite) should be considered simultaneously. Since the material properties are determined by the functional motifs and their arrangements synergistically, more construction structures, such as 3D/2D/3D/2D, or patterned 3D/2D, are encouraged to be explored.

(b) A deep study of the morphology of low-dimensional perovskites is needed. Most previous studies are based on routine techniques, which are actually not feasible for the ultrathin 2D layer that features with similar properties with the substrate (i.e. 3D perovskite). Some studies have shown that vertical crystal orientation of low-dimensional perovskite is more conducive to charge extraction. However, how to control the crystal orientation to grow along the vertical direction has not been fully investigated. In addition, the match of physical and chemical properties of these two layers, such as crystalline lattice, optical, carrier transfer is expected to be studied and designed. High throughput theoretical calculation and modulations are suggested to be involved.

(c) The deposition methods of the ammonium salt for low-dimensional perovskite are suggested to be scalable. The main reported strategy used for low-dimensional layer deposition is spin-coating, which is not feasible for mass production. More attention should be paid to the deposition of low-dimensional perovskite layers.

In addition, most research reports only provide the stability test data under one condition of humidity, temperature and light *etc*, which cannot reveal the stability of the device accurately and comprehensively. A standardized protocol for enhancing the long-term stability of perovskite cells and modules should be developed. With a successful transfer of the knowledge and merits of other technologies, such as CdTe solar cell, CIGS solar cells, OLED, along with a more dedicate module design, interface engineering, and composition engineering that is specific for perovskite PV technology, we believe that the present issues will be overcome in the coming years to help PSCs to be commercialized.

Acknowledgments

This work is financially supported by the National Natural Science Foundation of China (91963209, 52002302, 22075221 and 52102215), Foshan Xianhu Laboratory of the Advanced Energy Science and Technology Guangdong Laboratory (XHD2020-001), and the Fundamental Research Funds for the Central Universities (WUT: 2021IVB038 and 2021VA101). M H acknowledges the support from State Key Laboratory of Silicate Materials for Architectures (Wuhan University of Technology: SYSJJ2021-10).

Conflict of interest

The authors declare no competing financial interest.

ORCID iD

Jianfeng Lu https://orcid.org/0000-0001-5586-4656

References

[1] Green M A, Dunlop E D, Hohl-Ebinger J, Yoshita M, Kopidakis N and Hao X 2020 Solar cell efficiency tables (version 56) *Prog. Photovolt., Res. Appl.* **28** 629–38

[2] Cao Q, Li P, Chen W, Zang S, Han L, Zhang Y and Song Y 2022 Two-dimensional perovskites: impacts of species, components, and properties of organic spacers on solar cells *Nano Today* **43** 101394

[3] Bai Y, Dong Q, Shao Y, Deng Y, Wang Q, Shen L, Wang D, Wei W and Huang J 2016 Enhancing stability and efficiency of perovskite solar cells with crosslinkable silane-functionalized and doped fullerene *Nat. Commun.* **7** 1–9

[4] Mo Y *et al* 2022 Nitrogen-doped tin oxide electron transport layer for stable perovskite solar cells with efficiency over 23% *Interdiscip. Mater.* **1** 309–15

[5] Xie Y-M, Yao Q, Xue Q, Zeng Z, Niu T, Zhou Y, Zhuo M-P, Tsang S-W, Yip H-L and Cao Y 2022 Subtle side chain modification of triphenylamine-based polymer hole-transport layer materials produces efficient and stable inverted perovskite solar cells *Interdiscip. Mater.* **1** 281–93

[6] Bi D, Yi C, Luo J, Décoppet J-D, Zhang F, Zakeeruddin Shaik M, Li X, Hagfeldt A and Grätzel M 2016 Polymer-templated nucleation and crystal growth of perovskite films for solar cells with efficiency greater than 21% *Nat. Energy* **1** 1–5

[7] Kanda H *et al* 2022 Three-terminal perovskite/integrated back contact silicon tandem solar cells under low light intensity conditions *Interdiscip. Mater.* **1** 148–56

[8] Zheng X, Chen B, Dai J, Fang Y, Bai Y, Lin Y, Wei H, Zeng X and Huang J 2017 Defect passivation in hybrid perovskite solar cells using quaternary ammonium halide anions and cations *Nat. Energy* **2** 1–9

[9] Li Z, Yang M, Park J-S, Wei S-H, Berry J J and Zhu K 2015 Stabilizing perovskite structures by tuning tolerance factor: formation of formamidinium and cesium lead iodide solid-state alloys *Chem. Mater.* **28** 284–92

[10] Lin Y, Bai Y, Fang Y, Chen Z, Yang S, Zheng X, Tang S, Liu Y, Zhao J and Huang J 2018 Enhanced thermal stability in perovskite solar cells by assembling 2D/3D stacking structures *J. Phys. Chem. Lett.* **9** 654–8

[11] Wang Z, Lin Q, Chmiel F P, Sakai N, Herz L M and Snaith H J 2017 Efficient ambient-air-stable solar cells with 2D–3D heterostructured butylammonium-caesium-formamidinium lead halide perovskites *Nat. Energy* **2** 1–10

[12] Wu Y-H, Ding Y, Liu X-Y, Ding X-H, Liu X-P, Pan X and Dai S-Y 2019 Ambient stable $FAPbI_3$-based perovskite solar cells with a 2D-$EDAPbI_4$ thin capping layer *Sci. China Mater.* **63** 47–54

[13] Stoumpos C C and Kanatzidis M G 2016 Halide perovskites: poor man's high-performance semiconductors *Adv. Mater.* **28** 5778–93

[14] Lin L, Jones T W, Yang T C J, Duffy N W, Li J, Zhao L, Chi B, Wang X and Wilson G J 2020 Inorganic electron transport materials in perovskite solar cells *Adv. Funct.* **31** 2008300

[15] Zhao X, Liu T and Loo Y L 2022 Advancing 2D perovskites for efficient and stable solar cells: challenges and opportunities *Adv. Mater.* **34** e2105849

[16] Dou L *et al* 2015 Atomically thin two-dimensional organic-inorganic hybrid perovskites *Science* **349** 1518–21

[17] Quan L N *et al* 2016 Ligand-stabilized reduced-dimensionality perovskites *J. Am. Chem. Soc.* **138** 2649–55

[18] Lin H, Zhou C, Tian Y, Siegrist T and Ma B 2017 Low-dimensional organometal halide perovskites *ACS Energy Lett.* **3** 54–62

[19] Sun S, Lu M, Gao X, Shi Z, Bai X, Yu W W and Zhang Y 2021 0D perovskites: unique properties, synthesis, and their applications *Adv. Sci.* **8** e2102689

[20] Han Y, Yue S and Cui B B 2021 Low-dimensional metal halide perovskite crystal materials: structure strategies and luminescence applications *Adv. Sci.* **8** e2004805

[21] Castro-Méndez A F, Hidalgo J and Correa-Baena J P 2019 The role of grain boundaries in perovskite solar cells *Adv. Energy Mater.* **9** 149–60

[22] Chen P, Bai Y, Lyu M, Yun J-H, Hao M and Wang L 2018 Progress and perspective in low-dimensional metal halide perovskites for optoelectronic applications *Sol. RRL* **2** 1700186

[23] Zhu P and Zhu J 2020 Low-dimensional metal halide perovskites and related optoelectronic applications *InfoMat* **2** 341–78

[24] Yang S, Wang Y, Liu P, Cheng Y-B, Zhao H J and Yang H G 2016 Functionalization of perovskite thin films with moisture-tolerant molecules *Nat. Energy* **1** 1–7

[25] Etgar L 2018 The merit of perovskite's dimensionality; can this replace the 3D halide perovskite? *Energy Environ. Sci.* **11** 234–42

[26] Zhang F, Kim D H and Zhu K 2018 3D/2D multidimensional perovskites: balance of high performance and stability for perovskite solar cells *Curr. Opin. Electrochem.* **11** 105–13

[27] Yoo J J *et al* 2019 An interface stabilized perovskite solar cell with high stabilized efficiency and low voltage loss *Energy Environ. Sci.* **12** 2192–9

[28] Bai G, Wu Z, Li J, Bu T, Li W, Li W, Huang F, Zhang Q, Cheng Y-B and Zhong J 2019 High performance perovskite sub-module with sputtered SnO_2 electron transport layer *Sol. Energy* **183** 306–14

[29] Bu T *et al* 2017 A novel quadruple-cation absorber for universal hysteresis elimination for high efficiency and stable perovskite solar cells *Energy Environ. Sci.* **10** 2509–15

[30] Bu T, Liu X, Li J, Huang W, Wu Z, Huang F and Zhong J 2020 Dynamic antisolvent engineering for spin coating of 10×10 cm^2 perovskite solar module approaching 18% *Sol. RRL* **4** 1900263

[31] Bu T, Li J, Zheng F, Chen W, Wen X, Ku Z, Peng Y, Zhong J, Cheng Y-B and Huang F 2018 Universal passivation strategy to slot-die printed SnO_2 for hysteresis-free efficient flexible perovskite solar module *Nat. Commun.* **9** 4609

[32] Chiang C-H, Lin J-W and Wu C-G 2016 One-step fabrication of mixed-halide perovskite film for high-efficiency inverted solar cell and module *J. Mater.* **4** 13525–33

[33] Chiang C-H, Nazeeruddin M K, Grätzel M and Wu C-G 2017 The synergistic effect of H_2O and DMF towards stable and 20% efficiency inverted perovskite solar cells *Energy Environ. Sci.* **10** 808–17

[34] Cho Y, Soufiani A M, Yun J S, Kim J, Lee D S, Seidel J, Deng X, Green M A, Huang S and Ho-Baillie A W Y 2018 Mixed 3D-2D passivation treatment for mixed-cation lead mixed-halide perovskite solar cells for higher efficiency and better stability *Adv. Energy Mater.* **8** 1703392

[35] Dai X, Deng Y, Van Brackle C H, Chen S, Rudd P N, Xiao X, Lin Y, Chen B and Huang J 2019 Scalable fabrication of efficient perovskite solar modules on flexible glass substrates *Adv. Energy Mater.* **10** 1903108

[36] Deng Y, Van Brackle C H, Dai X, Zhao J, Chen B and Huang J 2019 Tailoring solvent coordination for high-speed, room-temperature blading of perovskite photovoltaic films *Sci. Adv.* **5** eaax7537

[37] Fakharuddin A D G F *et al* 2015 Vertical TiO_2 nanorods as a medium for durable and high efficiency perovskite solar modules *ACS Nano* **9** 8420–9

[38] Zhang F *et al* 2022 Metastable Dion–Jacobson 2D structure enables efficient and stable perovskite solar cells *Science* **375** 71–76

[39] Gotanda T, Oooka H, Mori S, Nakao H, Amano A, Todori K, Nakai Y and Mizuguchi K 2019 Facile and scalable fabrication of low-hysteresis perovskite solar cells and modules using a three-step process for the perovskite layer *J. Power Sources* **430** 145–9

[40] Green M A, Dunlop E D, Hohl-Ebinger J, Yoshita M, Kopidakis N and Hao X 2021 Solar cell efficiency tables (Version 58) *Prog. Photovolt., Res. Appl.* **29** 657–67

[41] Green M A, Dunlop E D, Levi D H, Hohl-Ebinger J, Yoshita M and Ho-Baillie A W Y 2019 Solar cell efficiency tables (version 54) *Prog. Photovolt., Res. Appl.* **27** 565–75

[42] Heo J H, Han H J, Kim D, Ahn T K and Im S H 2015 Hysteresis-less inverted $CH_3NH_3PbI_3$ planar perovskite hybrid solar cells with 18.1% power conversion efficiency *Energy Environ. Sci.* **8** 1602–8

[43] Heo J H, Lee M H, Jang M H and Im S H 2016 Highly efficient $CH_3NH_3PbI_{3-x}Cl_x$ mixed halide perovskite solar cells prepared by re-dissolution and crystal grain growth via spray coating *J. Mater.* **4** 17636–42

[44] Jeong J *et al* 2021 Pseudo-halide anion engineering for α-$FAPbI_3$ perovskite solar cells *Nature* **592** 381–5

[45] Jeong M *et al* 2020 Stable perovskite solar cells with efficiency exceeding 24.8% and 0.3-V voltage loss *Science* **369** 1615–20

[46] Jiang Y, Leyden M R, Qiu L, Wang S, Ono L K, Wu Z, Juarez-Perez E J and Qi Y 2018 Combination of hybrid CVD and cation exchange for upscaling cs-substituted mixed cation perovskite solar cells with high efficiency and stability *Adv. Funct.* **28** 1703835

[47] Jiang Y *et al* 2019 Negligible-Pb-waste and upscalable perovskite deposition technology for high-operational-stability perovskite solar modules *Adv. Energy Mater.* **9** 1803047

[48] Jung E H, Jeon N J, Park E Y, Moon C S, Shin T J, Yang T Y, Noh J H and Seo J 2019 Efficient, stable and scalable perovskite solar cells using poly (3-hexylthiophene) *Nature* **567** 511–5

[49] Kim M *et al* 2022 Conformal quantum dot–SnO_2 layers as electron transporters for efficient perovskite solar cells *Science* **375** 302–6

[50] Kim M *et al* 2019 Methylammonium chloride induces intermediate phase stabilization for efficient perovskite solar cells *Joule* **3** 2179–92

[51] Kwon H-C, Ma S, Yun S-C, Jang G, Yang H and Moon J 2020 A nanopillar-structured perovskite-based efficient semitransparent solar module for power-generating window applications *J. Mater.* **8** 1457–68

[52] Liao H-C *et al* 2017 Enhanced efficiency of hot-cast large-area planar perovskite solar cells/modules having controlled chloride incorporation *Adv. Energy Mater.* **7** 1601660

[53] Liu Z *et al* 2020 A holistic approach to interface stabilization for efficient perovskite solar modules with over 2000-hour operational stability *Nat. Energy* **5** 596–604

[54] Lou L, Liu T, Xiao J, Xiao S, Long X, Zheng S and Yang S 2019 Controlling apparent coordinated solvent number in the perovskite intermediate phase film for developing large-area perovskite solar modules *Energy Technol.* **8** 1900972

[55] NREL 2022 Best Research-Cell Efficiency Chart (available at: https://www.nrel.gov/pv/assets/pdfs/best-research-cell-efficiencies-rev220630.pdf) (Accessed October 2022)

[56] Priyadarshi A, Haur L J, Murray P, Fu D, Kulkarni S, Xing G, Sum T C, Mathews N and Mhaisalkar S G 2016 A large area (70 cm^2) monolithic perovskite solar module with a high efficiency and stability *Energy Environ. Sci.* **9** 3687–92

[57] Ren A *et al* 2020 Efficient perovskite solar modules with minimized nonradiative recombination and local carrier transport losses *Joule* **4** 1263–77

[58] Seo J, Park S, Chan Kim Y, Jeon N J, Noh J H, Yoon S C and Seok S I 2014 Benefits of very thin PCBM and LiF layers for solution-processed p–i–n perovskite solar cells *Energy Environ. Sci.* **7** 2642–6

[59] Smith I C, Hoke E T, Solis-Ibarra D, McGehee M D and Karunadasa H I 2014 A layered hybrid perovskite solar-cell absorber with enhanced moisture stability *Angew. Chem., Int. Ed. Engl.* **53** 11232–5

[60] Thi Kim C M, Atourki L, Ouafi M and Hashmi S G 2021 A synopsis of progressive transition in precursor inks development for metal halide perovskites-based photovoltaic technology *J. Mater.* **9** 26650–68

[61] Wang F, Geng W, Zhou Y, Fang H H, Tong C J, Loi M A, Liu L-M and Zhao N 2016 Phenylalkylamine passivation of organolead halide perovskites enabling high-efficiency and air-stable photovoltaic cells *Adv. Mater.* **28** 9986–92

[62] Yang M *et al* 2017 Perovskite ink with wide processing window for scalable high-efficiency solar cells *Nat. Energy* **2** 1–9

[63] Yao K, Wang X, Xu Y-X and Li F 2015 A general fabrication procedure for efficient and stable planar perovskite solar cells: morphological and interfacial control by *in-situ*-generated layered perovskite *Nano Energy* **18** 165–75

[64] Zhou Y, Wang F, Cao Y, Wang J-P, Fang H-H, Loi M A, Zhao N and Wong C-P 2017 Benzylamine-treated wide-bandgap perovskite with high thermal-photostability and photovoltaic performance *Adv. Energy Mater.* **7** 1701048

[65] Agresti A, Pescetelli S, Palma A L, Martín-García B, Najafi L, Bellani S, Moreels I, Prato M, Bonaccorso F and Di Carlo A 2019 Two-dimensional material interface engineering for efficient perovskite large-area modules *ACS Energy Lett.* **4** 1862–71

[66] Bi E *et al* 2019 Efficient perovskite solar cell modules with high stability enabled by iodide diffusion barriers *Joule* **3** 2748–60

[67] Bu T *et al* 2022 Modulating crystal growth of formamidinium–caesium perovskites for over 200 cm^2 photovoltaic sub-modules *Nat. Energy* **7** 528–36

[68] Castriotta L A, Fuentes Pineda R, Babu V, Spinelli P, Taheri B, Matteocci F, Brunetti F, Wojciechowski K and Di Carlo A 2021 Light-stable methylammonium-free inverted flexible perovskite solar modules on PET exceeding 10.5% on a 15.7 cm^2 active area *ACS Appl. Mater.* **13** 29576–84

[69] Gao W, Chao L, Li M, Xia Y, Ran C and Chen Y 2022 Ternary halogen doping for efficient and stable air-processed all-inorganic perovskite solar cells *Sol. RRL* **6** 2200457

[70] Grancini G *et al* 2017 One-year stable perovskite solar cells by 2D/3D interface engineering *Nat. Commun.* **8** 1–8

[71] Huang Z *et al* 2021 Releasing nanocapsules for high-throughput printing of stable perovskite solar cells *Adv. Energy Mater.* **11** 2101291

[72] Liu Y, Cao H, Liu X, Zhu R, Tao T and Sun J 2021 Fabricating efficient and stable quasi-3D and 3D/2D perovskite solar cells with 2D-sheets connected by inorganic type ionic-bond *Nanotechnology* **32** 355201

[73] Mei A *et al* 2020 Stabilizing perovskite solar cells to IEC61215:2016 standards with over 9 000-h operational tracking *Joule* **4** 2646–60

[74] Paek S *et al* 2020 Molecular design and operational stability: toward stable 3D/2D perovskite interlayers *Adv. Sci.* **7** 2001014

[75] Qiu L, Liu Z, Ono L K, Jiang Y, Son D Y, Hawash Z, He S and Qi Y 2018 Scalable fabrication of stable high efficiency perovskite solar cells and modules utilizing room temperature sputtered SnO_2 electron transport layer *Adv. Funct.* **29** 1806779

[76] Roß M *et al* 2021 Co-evaporated formamidinium lead iodide based perovskites with 1000 h constant stability for fully textured monolithic perovskite/silicon tandem solar cells *Adv. Energy Mater.* **11** 2101460

[77] Sánchez S *et al* 2022 Thermally controlled growth of photoactive $fapbi_3$ films for highly stable perovskite solar cells *Energy Environ. Sci.* **15** 3862–76

[78] Xiao K *et al* 2020 All-perovskite tandem solar cells with 24.2% certified efficiency and area over 1 cm^2 using surface-anchoring zwitterionic antioxidant *Nat. Energy* **5** 870–80

[79] Yang N *et al* 2020 An *in situ* cross-linked 1D/3D perovskite heterostructure improves the stability of hybrid perovskite solar cells for over 3000 h operation *Energy Environ. Sci.* **13** 4344–52

[80] Yang Z *et al* 2021 Slot-die coating large-area formamidinium-cesium perovskite film for efficient and stable parallel solar module *Sci. Adv.* **7** eabg3749

[81] Zhang Y *et al* 2020 The synergism of DMSO and diethyl ether for highly reproducible and efficient $MA_{0.5}FA_{0.5}PbI_3$ perovskite solar cells *Adv. Energy Mater.* **10** 2001300

[82] Deng Y, Xu S, Chen S, Xiao X, Zhao J and Huang J 2021 Defect compensation in formamidinium–caesium perovskites for highly efficient solar mini-modules with improved photostability *Nat. Energy* **6** 633–41

[83] Chen H *et al* 2022 Quantum-size-tuned heterostructures enable efficient and stable inverted perovskite solar cells *Nat. Photon.* **16** 352–8

[84] Bu T *et al* 2021 Lead halide–templated crystallization of methylamine-free perovskite for efficient photovoltaic modules *Science* **372** 1327–32

[85] Azmi R *et al* 2022 Damp heat–stable perovskite solar cells with tailored-dimensionality 2D/3D heterojunctions *Science* **376** 73–77

[86] Zhan Y, Yang F, Chen W, Chen H, Shen Y, Li Y and Li Y 2021 Elastic lattice and excess charge carrier manipulation in 1D–3D perovskite solar cells for exceptionally long-term operational stability *Adv. Mater.* **33** e2105170

[87] Mahmud M A *et al* 2019 Double-sided surface passivation of 3D perovskite film for high-efficiency mixed-dimensional perovskite solar cells *Adv. Funct.* **30** 1907962

[88] He M, Liang J, Zhang Z, Qiu Y, Deng Z, Xu H and Chen C C 2020 Compositional optimization of a 2D–3D heterojunction interface for 22.6% efficient and stable planar perovskite solar cells *J. Mater.* **8** 25831–41

[89] Kaneko R, Kanda H, Shibayama N, Sugawa K, Otsuki J, Islam A and Nazeeruddin M K 2021 Gradient 1D/3D perovskite bilayer using 4-tert-butylpyridinium cation for efficient and stable perovskite solar cells *Sol. RRL* **5** 2000791

[90] Ma C *et al* 2016 2D/3D perovskite hybrids as moisture-tolerant and efficient light absorbers for solar cells *Nanoscale* **8** 18309–14

[91] Cho K T *et al* 2018 Selective growth of layered perovskites for stable and efficient photovoltaics *Energy Environ. Sci.* **11** 952–9

[92] Bai Y, Xiao S, Hu C, Zhang T, Meng X, Lin H, Yang Y and Yang S 2017 Dimensional engineering of a graded 3D-2D halide perovskite interface enables ultrahigh voc enhanced stability in the p-i-n photovoltaics *Adv. Energy Mater.* **7** 1701038

[93] Wei M *et al* 2020 Combining efficiency and stability in mixed tin-lead perovskite solar cells by capping grains with an ultrathin 2D layer *Adv. Mater.* **32** e1907058

[94] Li M H *et al* 2018 Highly efficient 2D/3D hybrid perovskite solar cells via low-pressure vapor-assisted solution process *Adv. Mater.* **30** e1801401

[95] Lin D *et al* 2019 Stable and scalable 3D-2D planar heterojunction perovskite solar cells via vapor deposition *Nano Energy* **59** 619–25

[96] La-Placa M-G, Gil-Escrig L, Guo D, Palazon F, Savenije T J, Sessolo M and Bolink H J 2019 Vacuum-deposited 2D/3D perovskite heterojunctions *ACS Energy Lett.* **4** 2893–901

[97] Jang Y-W, Lee S, Yeom K M, Jeong K, Choi K, Choi M and Noh J H 2021 Intact 2D/3D halide junction perovskite solar cells via solid-phase in-plane growth *Nat. Energy* **6** 63–71

[98] Zhao D *et al* 2022 Efficient and stable 3D/2D perovskite solar cells through vertical heterostructures with $(BA)_4AgBiBr_8$ nanosheets *Adv. Mater.* **34** 2204661

[99] Zheng Y, Yang X, Su R, Wu P, Gong Q and Zhu R 2020 High-performance $CsPbI_xBr_{3-x}$ all-inorganic perovskite solar cells with efficiency over 18% via spontaneous interfacial manipulation *Adv. Funct.* **30** 2000457

[100] Xu X, Qian W, Wang J, Yang J, Chen J, Xiao S, Ge Y and Yang S 2021 Sequential growth of 2D/3D double-layer perovskite films with superior x-ray detection performance *Adv. Sci.* **8** e2102730

[101] Liu C *et al* 2021 Tuning structural isomers of phenylenediammonium to afford efficient and stable perovskite solar cells and modules *Nat. Commun.* **12** 6394

[102] Wang Y, Duan C, Lv P, Ku Z, Lu J, Huang F and Cheng Y-B 2021 Printing strategies for scaling-up perovskite solar cells *Natl Sci. Rev.* **8** nwab075

[103] Jung M, Ji S G, Kim G and Seok S I 2019 Perovskite precursor solution chemistry: from fundamentals to photovoltaic applications *Chem. Soc. Rev.* **48** 2011–38

[104] Patidar R, Burkitt D, Hooper K, Richards D and Watson T 2020 Slot-die coating of perovskite solar cells: an overview *Mater. Today Commun.* **22** 100808

[105] Eggers H, Schackmar F, Abzieher T, Sun Q, Lemmer U, Vaynzof Y, Richards B S, Hernandez-Sosa G and Paetzold U W 2019 Inkjet-printed micrometer-thick perovskite solar cells with large columnar grains *Adv. Energy Mater.* **10** 1903184

[106] Li Z, Klein T R, Kim D H, Yang M, Berry J J, van Hest M F A M and Zhu K 2018 Scalable fabrication of perovskite solar cells *Nat. Rev. Mater.* **3** 1–20

[107] Tavakoli M M, Gu L, Gao Y, Reckmeier C, He J, Rogach A L, Yao Y and Fan Z 2015 Fabrication of efficient planar perovskite solar cells using a one-step chemical vapor deposition method *Sci. Rep.* **5** 1–9

[108] Leyden M R, Lee M V, Raga S R and Qi Y 2015 Large formamidinium lead trihalide perovskite solar cells using chemical vapor deposition with high reproducibility and tunable chlorine concentrations *J. Mater.* **3** 16097–103

[109] Luo P, Liu Z, Xia W, Yuan C, Cheng J and Lu Y 2015 Uniform, stable, and efficient planar-heterojunction perovskite solar cells by facile low-pressure chemical vapor deposition under fully open-air conditions *ACS Appl. Mater.* **7** 2708–14

[110] Zendehdel M, Yaghoobi Nia N, Paci B, Generosi A and Di Carlo A 2022 Zero-waste scalable blade–spin coating as universal approach for layer-by-layer deposition of 3D/2D perovskite films in high-efficiency perovskite solar modules *Sol. RRL* **6** 2100637

[111] Liu Y *et al* 2019 Ultrahydrophobic 3D/2D fluoroarene bilayer-based water-resistant perovskite solar cells with efficiencies exceeding 22% *Sci. Adv.* **5** eaaw2543

[112] Cheng Q, Xia H, Li X, Wang B, Li Y, Zhang X, Zhang H, Zhang Y and Zhou H 2022 High-efficiency and stable perovskite solar cells enabled by low-dimensional perovskite surface modifiers *Sol. RRL* **6** 2100805

[113] Pham N D, Yang Y, Hoang M T, Wang T, Tiong V T, Wilson G J and Wang H 2020 1D pyrrolidinium lead iodide for efficient and stable perovskite solar cells *Energy Technol.* **8** 1900918

[114] Kim N K *et al* 2017 Investigation of thermally induced degradation in $CH_3NH_3PbI_3$ perovskite solar cells using *in-situ* synchrotron radiation analysis *Sci. Rep.* **7** 4645

[115] Sutanto A A, Szostak R, Drigo N, Queloz V I E, Marchezi P E, Germino J C, Tolentino H C N, Nazeeruddin M K, Nogueira A F and Grancini G 2020 *In situ* analysis reveals the role of 2D perovskite in preventing thermal-induced degradation in 2D/3D perovskite interfaces *Nano Lett.* **20** 3992–8

[116] Heo S *et al* 2019 Origins of high performance and degradation in the mixed perovskite solar cells *Adv. Mater.* **31** e1805438

[117] Wang J, Liu L, Chen S, Qi L, Zhao M, Zhao C, Tang J, Cai X, Lu F and Jiu T 2022 Growth of 1D nanorod perovskite for surface passivation in $FAPbI_3$ perovskite solar cells *Small* **18** e2104100

[118] Mahapatra A, Runjhun R, Nawrocki J, Lewinski J, Kalam A, Kumar P, Trivedi S, Tavakoli M M, Prochowicz D and Yadav P 2020 Elucidation of the role of guanidinium incorporation in single-crystalline $MAPbI_3$ perovskite on ion migration and activation energy *Phys. Chem. Chem. Phys.* **22** 11467–73
[119] Hoke E T, Slotcavage D J, Dohner E R, Bowring A R, Karunadasa H I and McGehee M D 2015 Reversible photo-induced trap formation in mixed-halide hybrid perovskites for photovoltaics *Chem. Sci.* **6** 613–7
[120] Rong Y, Hu Y, Mei A, Tan H, Saidaminov M I, Seok S I, McGehee M D, Sargent E H and Han H 2018 Challenges for commercializing perovskite solar cells *Science* **361** eaat8235
[121] Li N *et al* 2019 Cation and anion immobilization through chemical bonding enhancement with fluorides for stable halide perovskite solar cells *Nat. Energy* **4** 408–15
[122] Shao Y *et al* 2016 Grain boundary dominated ion migration in polycrystalline organic–inorganic halide perovskite films *Energy Environ. Sci.* **9** 1752–9
[123] Fu X *et al* 2021 Halogen-halogen bonds enable improved long-term operational stability of mixed-halide perovskite photovoltaics *Chem* **7** 3131–43
[124] He Y, Pan W, Guo C, Zhang H, Wei H and Yang B 2021 3D/2D perovskite single crystals heterojunction for suppressed ions migration in hard x-ray detection *Adv. Funct.* **31** 2104880
[125] Ye X, Cai H, Sun Q, Xu T, Ni J, Li J and Zhang J 2022 Organic spacer engineering in 2D/3D hybrid perovskites for efficient and stable solar cells *New J. Chem.* **46** 2837–45
[126] Niu T *et al* 2019 Interfacial engineering at the 2D/3D heterojunction for high-performance perovskite solar cells *Nano Lett.* **19** 7181–90
[127] Lv Y, Shi Y, Song X, Liu J, Wang M, Wang S, Feng Y, Jin S and Hao C 2018 Bromine doping as an efficient strategy to reduce the interfacial defects in hybrid two-dimensional/three-dimensional stacking perovskite solar cells *ACS Appl. Mater.* **10** 31755–64
[128] Elsenety M M, Antoniadou M, Balis N, Kaltzoglou A, Sygellou L, Stergiou A, Tagmatarchis N and Falaras P 2020 Stability improvement and performance reproducibility enhancement of perovskite solar cells following (FA/MA/Cs)$PbI_{3-x}Br_x$/$(CH_3)_3SPbI_3$ dimensionality engineering *ACS Appl. Energy Mater.* **3** 2465–77
[129] Ono L K, Liu S F and Qi Y 2020 Reducing detrimental defects for high-performance metal halide perovskite solar cells *Angew. Chem., Int. Ed. Engl.* **59** 6676–98
[130] Zhou L, Su J, Lin Z, Guo X, Ma J, Li T, Zhang J, Chang J and Hao Y 2021 Synergistic interface layer optimization and surface passivation with fluorocarbon molecules toward efficient and stable inverted planar perovskite solar cells *Research* **2021** 1–11
[131] Long M, Zhang T, Liu M, Chen Z, Wang C, Xie W, Xie F, Chen J, Li G and Xu J 2018 Abnormal synergetic effect of organic and halide ions on the stability and optoelectronic properties of a mixed perovskite via *in situ* characterizations *Adv. Mater.* **30** e1801562
[132] Jiang Q, Zhao Y, Zhang X, Yang X, Chen Y, Chu Z, Ye Q, Li X, Yin Z and You J 2019 Surface passivation of perovskite film for efficient solar cells *Nat. Photon.* **13** 460–6
[133] Galagan Y, Di Giacomo F, Gorter H, Kirchner G, de Vries I, Andriessen R and Groen P 2018 Roll-to-roll slot die coated perovskite for efficient flexible solar cells *Adv. Energy Mater.* **8** 1801935
[134] Li J *et al* 2018 Phase transition control for high-performance blade-coated perovskite solar cells *Joule* **2** 1313–30
[135] Cheng Y and Ding L 2021 Pushing commercialization of perovskite solar cells by improving their intrinsic stability *Energy Environ. Sci.* **14** 3233–55
[136] Park N-G and Zhu K 2020 Scalable fabrication and coating methods for perovskite solar cells and solar modules *Nat. Rev. Mater.* **5** 333–50
[137] Gao L, Chen L, Huang S, Li X and Yang G 2019 Series and parallel module design for large-area perovskite solar cells *ACS Appl. Energy Mater.* **2** 3851–9
[138] Kim D H, Whitaker J B, Li Z, van Hest M F A M and Zhu K 2018 Outlook and challenges of perovskite solar cells toward terawatt-scale photovoltaic module technology *Joule* **2** 1437–51
[139] Moon S-J, Yum J-H, Lofgren L, Walter A, Sansonnens L, Benkhaira M, Nicolay S, Bailat J and Ballif C 2015 Laser-scribing patterning for the production of organometallic halide perovskite solar modules *IEEE J. Photovolt.* **5** 1087–92
[140] Wilkinson B, Chang N L, Green M A and Ho-Baillie A W Y 2018 Scaling limits to large area perovskite solar cell efficiency *Prog. Photovolt.* **26** 659–74
[141] Rakocevic L, Mundt L E, Gehlhaar R, Merckx T, Aernouts T, Schubert M C, Glunz S W and Poortmans J 2019 Loss analysis in perovskite photovoltaic modules *Sol. RRL* **3** 1900338
[142] Kim J Y *et al* 2022 *In situ* formation of Imidazole-Based 2D interlayer for efficient perovskite solar cells and modules *Int. J. Energy Res.* **46** 15419–27
[143] Ma X, Pan J, Wang Y, Gao X, Hu M, Ku Z, Ma Y, Huang F, Cheng Y-B and Lu J 2022 Bromide complimented methylammonium-free wide bandgap perovskite solar modules with high efficiency and stability *Chem. Eng. J.* **445** 136626
[144] Xu Z, Chen R, Wu Y, He R, Yin J, Lin W and Zheng N 2019 Br-containing alkyl ammonium salt-enabled scalable fabrication of high-quality perovskite films for efficient and stable perovskite modules *J. Mater.* **7** 26849–57
[145] Xiao K *et al* 2022 Scalable processing for realizing 21.7%-efficient all-perovskite tandem solar modules *Science* **376** 762–7
[146] Jiang L, Lu J, Raga S R, Sun J, Lin X, Huang W, Huang F, Bach U and Cheng Y-B 2019 Fatigue stability of $CH_3NH_3PbI_3$ based perovskite solar cells in day/night cycling *Nano Energy* **58** 687–94
[147] Razera R A Z *et al* 2020 Instability of p–i–n perovskite solar cells under reverse bias *J. Mater.* **8** 242–50